Report LR-643

The behaviour of flux-difference and flux-vector splitting methods in explicit schemes for hypersonic blunt body flow

September 1990

A.C.J. Venis

TU Delft
Delft University of Technology

Faculty of Aerospace Engineering

report LR-643

The behaviour of flux-difference and flux-vector splitting methods in explicit schemes for hypersonic blunt body flow

September 1990

A.C.J. Venis

TUDelft Faculty of Aerospace Engineering

Summary

A survey of the behaviour of flux difference and flux-vector splitting methods is given. The schemes of Roe, van Leer, and Hänel are examined for a two-dimensional, inviscid, hypersonic blunt body flow of a perfect gas. It appears that on fine meshes Roe's scheme is not enough dissipative to sufficiently damp errors in the solution. A modified entropy correction with a properly dosed amount of numerical viscosity is needed to avoid the generation of physically unrealistic solutions and to provide convergence on fine meshes. The schemes of van Leer and Hänel perform well on the fine meshes. The Hänel scheme offers a better preservation of total enthalpy. For the present test problem, the use of the critical speed of sound in the scheme of Hänel could not be confirmed to be more appropriate than the static speed of sound used in van Leer's original scheme. Difficulties related to the incorrect calculation of thermodynamic quantities existed at high CFL numbers less than one where the integration scheme becomes unstable. All three numerical flux formulations exhibit this behaviour. The present results do not withstand the experience as reported by other authors.

Table of Contents

1 Introduction

The development of hypervelocity airplanes requires knowledge about the behaviour of the flow over such vehicles. Free flight experiments are very costly to realize. Wind tunnel experiments introduce scale effects in the flow which generate significant differences with the results obtained from inflight experiments. Computational fluid dynamics provides a powerful tool in order to fill the gap between the free flight and wind tunnel experiments. Consequently, robust, accurate and efficient numerical methods to calculate the flow fields of interest must become available.

Earlier CFD research of the author [1] on the hypersonic flow through quasi one-dimensional nozzles revealed some unfavourable properties of one of the commonly used numerical schemes, the flux difference splitting scheme due to Roe. It is the object of this report to shed some light on the behaviour of flux difference and flux-vector splitting methods in explicit schemes for solving hypersonic flow problems. Difficulties in using the flux difference schemes in the hypersonic flow regime have also been reported in [2], [3], and [4].

Here, we will discuss the flux difference scheme of Roe, the original flux-vector splitting scheme due to van Leer, and the modified van Leer scheme by Hänel. All of the above mentioned schemes have some specific properties which will be considered. We will examine the behaviour of the schemes on a two-dimensional, inviscid, hypersonic blunt body flow of a perfect gas at Mach 10.

The flow field will contain a very strong detached bow shock wave which is to be captured accurately by the numerical flux schemes. In hypersonic flow the severe strength of the shock waves and the manner in which they develop into a steady state shock in the numerical simulation of the problem, can cause some hard difficulties in correctly solving the flow problem. Furthermore, the splitting schemes show a dependency on certain flow properties that are difficult to obtain accurately in hypervelocity flows.

The reason for the choice of hypersonic, inviscid blunt body flow of a perfect gas as a test problem is simplicity. Perfect gas computer codes are faster than codes for real gases. Moreover, for the object of this work it is sufficient to consider the schemes for a perfect gas in the hypersonic flow regime. Several generalizations of the numerical flux schemes for gases obeying an arbitrary equation of state can be found in the literature. However, some significant quantities, such as the speed of sound, become slightly ambiguous to determine. Thus, extra difficulties would be introduced without contributing to the heart of the matter to be discussed here.

Therefore, we will compute the two-dimensional inviscid, steady state hypersonic flow past a hyperbola at Mach 10 with zero angle of attack. This will be done by solving the time dependent Euler equations of motion. The steady state solution is achieved by an explicit time integration scheme. The marching is in a time-like fashion where the time steps are locally determined.

In the next section, the governing equations to be solved and a discussion of the numerical flux schemes are given. In section 3 the hyperbola test problem is completely specified. Section 4 contains a discussion of the numerical results. In section 5 some final conclusions are drawn.

2 Numerical schemes for the Euler equations

2.1 Equations governing hypersonic perfect gas flow

The inviscid, hypersonic flow of a perfect gas is governed by the Euler equations of motion. The equations for two-dimensional flow will be used in their conservative form.

$$\frac{\partial q}{\partial t} + \frac{\partial f(q)}{\partial x} + \frac{\partial g(q)}{\partial y} = 0 \tag{2.1}$$

In eq.(2.1) q is the state vector, f and g are flux vectors, according to:

$$\begin{aligned} q &= (\rho, \rho u, \rho v, E)^T \\ f(q) &= (\rho u, \rho u^2 + p, \rho uv, (E+p)u)^T \\ g(q) &= (\rho v, \rho uv, \rho v^2 + p, (E+p)v)^T \end{aligned} \tag{2.2}$$

where ρ is the gas' density, u and v are the velocity components in $x-$ and $y-$ direction, respectively, p is the pressure and E the total energy. The gas is assumed to be calorically perfect, thus the equation of state reads

$$p = (\gamma - 1)\rho e \tag{2.3}$$

with γ the ratio of specific heats (c_p / c_v). The internal energy e is related to temperature T as

$$e = c_v T \tag{2.4}$$

Equations (2.1), (2.3) and (2.4) fully describe the two-dimensional inviscid hypersonic perfect gas flow.

2.2 Numerical approach

The governing conservation laws eq.(2.1) are numerically solved by an upwind, cell-centered finite volume method on a structured two-dimensional mesh. (fig. 2.1)

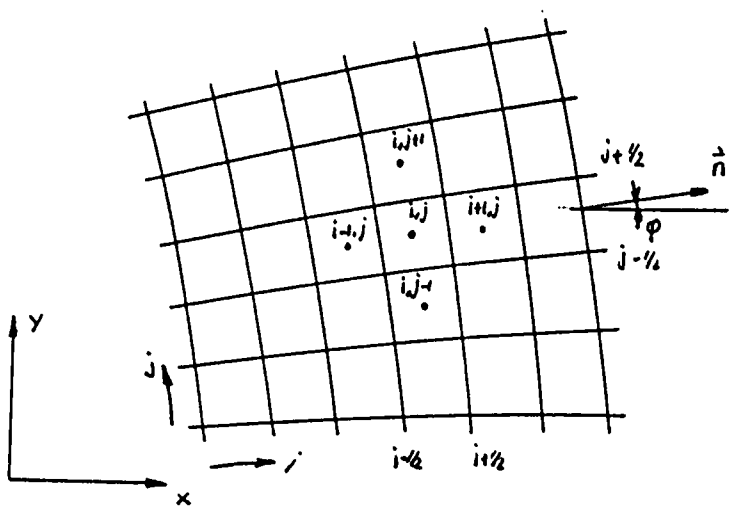

Fig. 2.1 Structured 2D mesh

An extensive discussion of the finite volume formulation can be found in [5]. Here, we will only briefly discuss the numerical formulation.

By expressing the conservation laws in their integral form, the finite volume approach becomes apparent. A formal discretization on a 2D mesh reads

$$\frac{dq_{i,j}}{dt} = -\frac{1}{V_{i,j}} \int_{\partial\Omega_{i,j}} (f\cos\phi + g\sin\phi)\, d\sigma \tag{2.5}$$

where $q_{i,j}$ denotes the state in a volume (or cell) $\Omega_{i,j}$. $V_{i,j}$ represents the volume of $\Omega_{i,j}$, $\partial\Omega_{i,j}$ the boundary of $\Omega_{i,j}$ and ϕ is the angle between the outward facing normal to $\partial\Omega_{i,j}$ and the x-axis in the fixed frame. By using the rotational invariance of the Euler equations, eq.(2.5) can be written as:

$$\frac{dq_{i,j}}{dt} = -\frac{1}{V_{i,j}} \int_{\partial\Omega_{i,j}} T^{-1}(\phi) f(T(\phi) q)\, d\sigma \tag{2.6}$$

where $T(\phi)$ is the transformation matrix, which transforms the state to a xy-frame with the x-axis normal to a cell interface and the y-axis aligned with the cell interface. It is defined as

$$\begin{pmatrix} 1 & 0 & 0 & 0 \\ 0 & \cos(\phi) & \sin(\phi) & 0 \\ 0 & -\sin(\phi) & \cos(\phi) & 0 \\ 0 & 0 & 0 & 1 \end{pmatrix} \tag{2.7}$$

The spatial discretization depends on the way in which the integral in the right-hand side of eq.(2.6) is evaluated. On a structured mesh consisting of quadrilateral volumes (as in fig. 2.1) the fluxes must be determined on each of the four cell interfaces.

By taking the states in cell centres as piece-wise constant data, or linearly, or non-linearly interpolated data, we arrive at a 1D Riemann problem for every cell interface:

$$\frac{\partial \tilde{q}}{\partial t} + \frac{\partial f(\tilde{q})}{\partial \tilde{x}} = 0$$

$$\tilde{q}(0,t) = \begin{cases} \tilde{q}^L & \tilde{x} < 0 \\ \tilde{q}^R & \tilde{x} > 0 \end{cases} \tag{2.8}$$

In eq.(2.8) $\tilde{x}$ denotes the x-axis of the local frame perpendicular to the cell interface. $\tilde{q}$ is the transformed state, $\tilde{q}^L$ and $\tilde{q}^R$ are the states, respectively to the left and to the right of the cell interface. In this way, an upwind discretization is obtained.

In this report we will consider two ways of tackling the above Riemann problem in order to obtain the fluxes on the cell interfaces. One way is based upon the discrimination between contributions of left and right moving waves to the flux difference over the cell interface: flux difference splitting (e.g. [6]). Another way is based on a velocity distribution of pseudo-particles and accounts for transport of properties (fluxes) from either the left or the right side of the cell interface: flux-vector splitting (e.g. [7]).

Both methods eventually yield a numerical flux function or approximate Riemann solver, $f_R(q^L, q^R)$. The accuracy of the discretization is determined by the way in which the left and right states are determined, see [1].

Using the numerical flux function $f_R(q^L, q^R)$ we can give a first order semi-discretization of the Euler equations on a two-dimensional mesh:

$$\begin{aligned}\frac{dq_{i,j}}{dt} = -\frac{1}{V_{i,j}}\{ & l_{i+\frac{1}{2},j}T^{-1}\left(\phi_{i+\frac{1}{2},j}\right)f_R\left(T\left(\phi_{i+\frac{1}{2},j}\right)q_{i,j}, T\left(\phi_{i+\frac{1}{2},j}\right)q_{i+1,j}\right) \\ & + l_{i,j+\frac{1}{2}}T^{-1}\left(\phi_{i,j+\frac{1}{2}}\right)f_R\left(T\left(\phi_{i,j+\frac{1}{2}}\right)q_{i,j}, T\left(\phi_{i,j+\frac{1}{2}}\right)q_{i,j+1}\right) \\ & - l_{i-\frac{1}{2},j}T^{-1}\left(\phi_{i-\frac{1}{2},j}\right)f_R\left(T\left(\phi_{i-\frac{1}{2},j}\right)q_{i,j}, T\left(\phi_{i-\frac{1}{2},j}\right)q_{i-1,j}\right) \\ & - l_{i,j-\frac{1}{2}}T^{-1}\left(\phi_{i,j-\frac{1}{2}}\right)f_R\left(T\left(\phi_{i,j-\frac{1}{2}}\right)q_{i,j}, T\left(\phi_{i,j-\frac{1}{2}}\right)q_{i,j-1}\right)\}\end{aligned} \tag{2.9}$$

In the following sections we will discuss the actual form of the numerical flux function and the time integration scheme.

2.3 Flux difference splitting; the Roe scheme

The term flux difference splitting becomes apparent when we consider the flux on a cell interface, denoted by $f_R(q^L, q^R)$, in terms of flux differences over the cell interface:

$$f_R(q^L, q^R) = \frac{1}{2}\{f(q^L) + f(q^R)\} - \frac{1}{2}\{\Delta f^+ - \Delta f^-\} \tag{2.10}$$

where

$$\begin{aligned}\Delta f^- &= f_R(q^L, q^R) - f(q^L) \\ \Delta f^+ &= f(q^R) - f_R(q^L, q^R)\end{aligned} \tag{2.11}$$

In [6] Roe suggested to take an average Jacobian matrix $\tilde{A}(q^L, q^R)$ of the Jacobian $A = df(q)/dq$ obeying what he called "Property U". Property U embodies

U1. $\tilde{A}(q^L, q^R) = A(q) = \frac{df(q)}{dq}$ *when* $q^L \to q^R \to q$

U2. $\Delta f = \tilde{A}\Delta q$ *with* $\Delta(.) = (.)^R - (.)^L$

U3. $\tilde{A}$ *has a set of linearly independent eigenvectors* $\tilde{R}_i$

For a perfect gas, Roe defined so-called Roe averages (further referred to by tilded quantities except where noted otherwise) according to

$$\begin{aligned}\tilde{\phi} &= \theta\phi^L + (1-\theta)\phi^R \\ \theta &= \frac{\sqrt{\rho^L}}{\sqrt{\rho^L} + \sqrt{\rho^R}} \\ \tilde{\rho} &= \sqrt{\rho^L \rho^R}\end{aligned} \tag{2.12}$$

where ϕ may be an arbitrary function. With the above definitions and "Property U" Roe derived a numerical flux function.

From U3 we find that Δq may be written on a basis of the eigenvectors $\tilde{R}_i$. For the Euler equations we get

$$\Delta q = \sum_{i=1}^{4} \tilde{\alpha}_i \tilde{R}_i \tag{2.13}$$

where $\tilde{\alpha}_i$ denotes the strength of the wave contributing to Δq. Then it follows from U2 that

$$\Delta f = \sum_{i=1}^{4} \tilde{\alpha}_i \tilde{\lambda}_i \tilde{R}_i \tag{2.14}$$

where $\tilde{\lambda}_i$ are the eigenvalues corresponding to the eigenvectors $\tilde{R}_i$.

The introduction of eq.(2.14) in the flux difference splitting scheme (eq.(2.11)) leads to

$$\begin{aligned} \Delta f^+ &= \sum_{i=1}^{4} \tilde{\alpha}_i \tilde{\lambda}_i^+ \tilde{R}_i, \qquad \tilde{\lambda}_i^+ = \max(0, \tilde{\lambda}_i) \\ \Delta f^- &= \sum_{i=1}^{4} \tilde{\alpha}_i \tilde{\lambda}_i^- \tilde{R}_i, \qquad \tilde{\lambda}_i^- = \min(0, \tilde{\lambda}_i) \end{aligned} \tag{2.15}$$

Substitution of eq.(2.15) in the numerical flux function $f_R(q^L, q^R)$ according to eq.(2.10) yields:

$$f_R(q^L, q^R) = \frac{1}{2}\{f(q^L) + f(q^R)\} - \frac{1}{2}\left\{\sum_{i=1}^{4} \tilde{\alpha}_i |\tilde{\lambda}_i| \tilde{R}_i\right\} \tag{2.16}$$

Writing the above flux function for the Euler equations in an alternative form (see also [1]), we arrive at

$$\begin{aligned} f_R(q^L, q^R) = \frac{1}{2}\{f(q^L) + f(q^R) - [&|\tilde{u}|\Delta q + (|\tilde{u} - \tilde{a}| - |\tilde{u}|)\tilde{\alpha}_1 \tilde{R}_1 \\ &(|\tilde{u} + \tilde{a}| - |\tilde{u}|)\tilde{\alpha}_2 \tilde{R}_2]\} \end{aligned} \tag{2.17}$$

with

$$\begin{aligned} \tilde{\alpha}_1 &= \frac{\Delta p - \tilde{\rho}\tilde{a}\Delta u}{2\tilde{a}^2} \\ \tilde{\alpha}_2 &= \frac{\Delta p + \tilde{\rho}\tilde{a}\Delta u}{2\tilde{a}^2} \\ \tilde{R}_1 &= (1, \tilde{u} - \tilde{a}, \tilde{v}, \tilde{H} - \tilde{u}\tilde{a})^t \\ \tilde{R}_2 &= (1, \tilde{u} + \tilde{a}, \tilde{v}, \tilde{H} + \tilde{u}\tilde{a})^t \end{aligned} \tag{2.18}$$

where $\tilde{a}$ is the Roe average of the speed of sound, defined as

$$\tilde{a}^2 = (\gamma - 1)\left\{\tilde{H} - \frac{1}{2}(\tilde{u}^2 + \tilde{v}^2)\right\} \tag{2.19}$$

$\tilde{H}$ is the Roe average of the total enthalpy $H = (E + p)/\rho$.

It can be shown (see [1]) that the scheme captures steady shock waves with at most one interior zone (volume). Furthermore, it is well known that the scheme eq.(2.17) is not consistent with an entropy inequality (see [6]). As a result, the scheme may capture unphysical discontinuities like expansion shocks. This can easily be repaired by means of an entropy correction, a so-called entropy-fix which in fact is a form of adding numerical viscosity to sonic points and shocks (see [4]). Further on, we will see that a correction on points

where the velocity $\tilde{u}$ vanishes is necessary also. The entropy-fix actually smoothes the transition of the eigenvalues occurring in the Roe scheme near shocks and sonic points, and, with the last modification, at points with zero velocity normal to the cell interface.

2.4 Flux-vector splitting; the van Leer scheme

The easiest way to achieve upwinding in the spatial discretization is by means of flux-vector splitting. In that case, the flux at a cell interface consists of the contribution from the flux from the left or from the right of the cell interface, according to the sign of the eigenvalues of the Jacobian $A(q) = df(q)/dq$.

The splitting is written as

$$f_R(q^L, q^R) = f^+(q^L) + f^-(q^R) \tag{2.20}$$

where f_R denotes the total flux, f^+ and f^- the contributions of the right and left moving pseudo-particles, respectively.

Here, we will discuss the original splitting according to van Leer [7]. We consider the fluxes in x-direction (locally normal to a cell interface) of the two-dimensional Euler equations for a perfect gas:

$$f(q) = \begin{pmatrix} \rho u \\ \rho u^2 + p \\ \rho uv \\ (E+p)u \end{pmatrix} = \begin{pmatrix} f_1 \\ f_2 \\ f_3 \\ f_4 \end{pmatrix} \tag{2.21}$$

and we wish to write them in terms of the density ρ, the static speed of sound a, and the local Mach number $M = u/a$, as follows

$$f(\rho, a, M, v) = \begin{pmatrix} \rho a M \\ \rho a^2\left(M^2 + \frac{1}{\gamma}\right) \\ \rho a M v \\ \rho a^3 M\left(\frac{1}{2}M^2 + \frac{1}{\gamma - 1}\right) \end{pmatrix} \tag{2.22}$$

where the static speed of sound is defined by:

$$a^2 = \gamma \frac{p}{\rho} \tag{2.23}$$

Van Leer suggested the following flux-vector splitting

$$f_R(q^L, q^R) = \begin{cases} f(q^R) & M \le -1 \\ \left[\begin{array}{l} f_1^+ = \pm\frac{\rho a}{4}(M \pm 1)^2 \\ f_2^+ = f_1^+\left\{\frac{(\gamma-1)u \pm 2a}{\gamma}\right\} \\ f_3^+ = f_1^+ v \\ f_4^+ = f_1^+\left\{\frac{[(\gamma-1)u \pm 2a]^2}{2(\gamma^2-1)}\right\} \end{array}\right] & |M| < 1 \\ f(q^R) & M \ge 1 \end{cases} \tag{2.24}$$

With this splitting we obtain a continuous numerical flux function that is also continuously differentiable. Furthermore, the formulation is such that one eigenvalue, the one that might adopt the wrong sign near sonic points and shock waves, vanishes for $|M| < 1$. This results in a smooth transition of the flux near sonic points, shock waves and points where the velocity normal to the cell interface vanishes. Also the vanishing eigenvalue provides a shock-capturing capability of steady shock waves with at most two interior zones (volumes). For proof, see [7] or [5].

Since the scheme does not connect two adjacent states by a discontinuity an entropy-fix is not appropriate. An unphysical expansion discontinuity will be recognized by the scheme to be broken down into the correct fan-like structure ([6]). As was the case with the flux difference scheme, the preservation of total enthalpy is not correct.

Another aspect of the van Leer splitting, although it is not an issue here, is the unfavourable resolution of contact discontinuities. This is due to the diffusive character of the flux-vector splitting method. However, this can be repaired as is shown by Hänel [3].

2.5 Flux-vector splitting; Hänel's modification of the van Leer scheme

One of the drawbacks of the original van Leer flux splitting scheme is the non-preservation of total enthalpy. It may lead to anomalous stagnation temperatures. Hänel [2,8] suggests therefore to replace the split energy flux by a split flux using the total enthalpy:

$$f_4^* = f_1^* H_t \tag{2.25}$$

where H_t is total enthalpy. Eq.(2.25) represents the transport of total enthalpy by the split mass fluxes f_1^* for $|M| < 1$. Thus, the transport of total enthalpy is correct for the entire range of Mach numbers, subsonic as well as supersonic in both directions.

Another drawback of the flux splitting scheme that may become apparent in high Mach number flows, is the dependence of the total flux on the static speed of sound. Especially in the hypervelocity range the calculation of the static speed of sound may become erroneous. It is calculated from the difference of total energy and kinetic energy, which are large values in hypervelocity flows wherein strong shock waves or strong expansions occur. As a result, the difference may become very small and faulty. Also other thermodynamic quantities like pressure, density and temperature may be quite strongly affected. Unphysical negative values can occur.

In order to avoid the dependency of the total flux on static speed of sound, as in the original van Leer splitting, the split fluxes are formulated as

$$\begin{aligned} f_1^* &= \pm \frac{\rho \hat{a}}{4}\left(\frac{u}{\hat{a}} \pm 1\right)^2 \\ f_2^* &= f_1^*\left[u - \frac{p}{\rho \hat{a}}\left(\frac{u}{\hat{a}} \mp 2\right)\right] \\ f_3^* &= f_1^* v \\ f_4^* &= f_1^* H_t \end{aligned} \tag{2.26}$$

The formulation eq.(2.26) was also given by Hänel [8] though it contained an error in the split x-momentum flux. The speed of sound $\hat{a}$ in eq.(2.26) can actually be chosen arbitrary. The only restriction to be imposed on $\hat{a}$ is that it must be equal to the static speed of sound in sonic points. A proper choice for $\hat{a}$ according to Hänel [3] is the critical speed of sound a^*. Thus

$$\hat{a} = a^* = \sqrt{\frac{2(\gamma+1)}{\gamma-1} H_t} \tag{2.27}$$

The total enthalpy H_t is a less varying quantity in viscous flow and a constant in steady Euler flow. As a result, together with a correct preservation of total enthalpy, the probability of a more correct calculation will be increased.

2.6 Implementation of a flux-vector splitting scheme using *sign*-functions

In order to be able to achieve an efficient computer code with a maximum degree of vectorization, it is recommendable to avoid the application of decision branches in the loops where the fluxes on the cell interfaces are to be calculated. Therefore, the numerical flux function of the flux-vector splitting will be given using *sign*-functions.

The schematic form of a flux-vector splitting scheme reads

$$f_R(q^L, q^R) = \begin{cases} f(q^R) & M \le -1 \\ f^+(q^L) + f^-(q^R) & |M| < 1 \\ f(q^L) & M \ge 1 \end{cases} \tag{2.28}$$

By defining the following functions

$$\begin{aligned} \alpha_L &= sign(1, M_L - 1), \qquad \alpha_R = sign(1, -(M_R + 1)) \\ \beta_L &= sign(1, |M_L| - 1), \qquad \beta_R = sign(1, |M_R| - 1) \end{aligned} \tag{2.29}$$

the numerical flux function becomes

$$f_R(q^L, q^R) = \frac{1+\alpha_L}{2} f(q^L) + \frac{1-\beta_L}{2} f^+(q^L) + \frac{1+\alpha_R}{2} f(q^R) + \frac{1-\beta_R}{2} f^-(q^R) \tag{2.30}$$

The above formulation can be applied to both the van Leer splitting scheme as well as to Hänel's modified splitting scheme.

2.7 The time integration scheme

We wish to solve the conservation laws for a steady state solution. To do so, the conservation laws are numerically integrated in time from $t = 0$ to $t \to \infty$. The integration scheme used for this purpose is the simple forward Euler scheme.

Consider the semi-discretization of the conservation laws on a two-dimensional mesh:

$$\frac{dq_{i,j}(t)}{t} = -\frac{\hat{F}_{i,j}}{V_{i,j}} \tag{2.31}$$

where $\hat{F}_{i,j}$ denotes the spatial discretization as given by eq.(2.9). The forward Euler scheme follows as

$$\Delta q^n_{i,j} = q^{n+1}_{i,j} - q^n_{i,j} = -\frac{\Delta t^n_{i,j}}{V_{i,j}} \hat{F}^n_{i,j} \tag{2.32}$$

where the superscript n denotes the time level. The time step $\Delta t^n_{i,j}$ is locally determined by a CFL condition at a constant CFL number for the entire mesh, such that we obtain a stable integration scheme. Thus, for two dimensions:

$$\Delta t^n_{i,j} \leq \frac{CFL}{\left(\frac{|u|+a}{\Delta x} + \frac{|v|+a}{\Delta y}\right)^n_{i,j}} \tag{2.33}$$

The maximum CFL number to be taken in actual computations is as large as 0.6.

A more sophisticated way of integrating the conservation laws with respect to time is achieved by applying a string of predictor-corrector methods, the so-called multi-stage integration schemes (see e.g. [1]). In doing so, a faster convergence can be achieved when local time step determination is applied. Also, a larger CFL number may be used, theoretically up to 1.5 for explicit schemes. In case of time accurate integration the scheme becomes second-order accurate in time.

3 Definition of a test case: MBB-hyperbola

The numerical schemes are tested on a two-dimensional hypersonic ($M\alpha = 10, \alpha = 0°$) blunt body flow problem. The blunt body geometry is a hyperbola as defined by MBB [9,10]. The definition of the test case is cited here for completeness.

MBB hyperbola geometry:

$$\left(\frac{x+500}{500}\right)^2 - \left(\frac{y}{88}\right)^2 = 1 \qquad (3.1)$$

where x and y are in mm.

The free stream flow conditions are defined as:

$$v_\infty = 2.975 \quad kms^{-1}$$
$$h \sim 52 \quad km$$
$$p_\infty = 48.67 \quad Pa$$
$$\rho_\infty = 7.7 \cdot 10^{-4} \quad kgm^{-3}$$
$$M_\infty = 10.006$$
$$Re/m = 1.6 \cdot 10^5 \quad m^{-1}$$

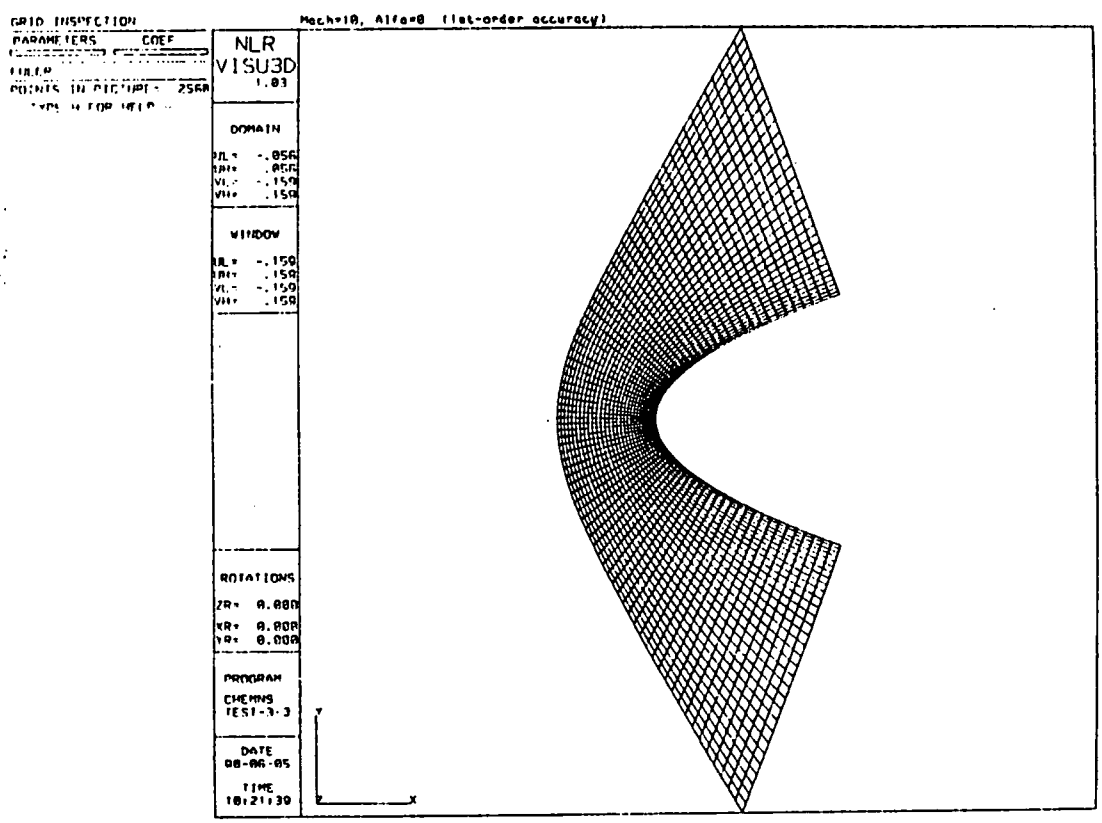

Fig. 3.1 Hyperbola geometry and 2D-mesh

4 Discussion of numerical results

We have solved the steady flow over the hyperbola as defined in section 3 using the numerical method as outlined in section 2. The solutions were obtained using each of the three numerical flux functions in a first-order approximation. The actual computations were performed on the NLR NEC-SX2 supercomputer sited at NLR-NOP.

The problem has been solved on several meshes varying in coarseness only. The computations using the van Leer splitting, and Hänel's modification have been performed on a 80x32-, a 160x64-, and a 320x128-mesh. The meshes were structured and the y-coordinates of the centres of the volumes were equi-distantly distributed. The computations using the Roe scheme have been performed on coarser meshes as well.

Fig. 4.1 shows a Mach contour plot of the solution on the 80x32 grid with the van Leer splitting. The results agree with the expectations of an inviscid perfect gas flow about a hyperbola at hypersonic Mach number. The contours qualitatively agree with the results given by MBB. The plot clearly shows a curved detached bow shock wave which is relatively close to the body surface. An interesting feature is the value of the stagnation temperature at the nose. The computed value appears to be $T_t = 4823\,K$ while the theoretical stagnation temperature based on the assumption of isenthalpic flow is found to be: $T_t = 4624.9\,K$. The numerical results show a violation of this assumption of isenthalpic flow. Fig. 4.2 shows the total enthalpy along the stagnation streamline. It is clear that the preservation of total enthalpy is not satisfied in the first-order computations using the van Leer scheme. Especially in the vicinity of the shock wave the loss, and downstream the gain of total enthalpy is very clear. This results in the higher stagnation temperature.

The shock is captured in two interior zones as shown by fig. 4.3. Compared to the result for inviscid perfect gas flow as given by MBB [9,10], the shock stand-off distance (fig. 4.3) seems to be in reasonable agreement. (x/r=0.583 and x/r=0.551 according to MBB, where r is the nose radius, r=1.5438 cm).

A computation with the van Leer scheme performed on the 160x64 grid (comparable to the grid used by MBB) shows almost no relevant differences in the Mach contours (fig. 4.4). Examination of the stagnation temperature yields $T_t = 4754.4\,K$ which is significantly lower than on the coarse mesh. The grid refinement has the expected result of a decrease of the stagnation temperature in the direction of the theoretical value. The vector plot of the nose region shows a reasonable numerical treatment of the inviscid boundary conditions (fig. 4.5). It also seems that the preservation of total enthalpy is improved by the grid refinement (fig. 4.6). The shock wave has moved in the direction of the body to x/r=0.551, perfectly comparable with the results from MBB. It is expected that further refinement improves the accuracy while the qualitative picture will not change any further.

The solution procedure did not show any unrobustness for this problem using the van Leer splitting. The initial CFL number was substantially lower than allowed according to the stability criterion. However, in order to obtain a neat start from an initially uniform solution, the CFL number is increased step-wise during

the integration process until a value of 0.6 is reached. A fast convergence is achieved on both the 80x32 and the 160x64 grid (figs. 4.7, 4.8). The consumed CPU-time per 1000 integration steps is 11 secs on the 80x32 mesh and 32 secs on the 160x64 mesh.

When we examine the solution of the same problem on the 80x32-mesh, obtained with Hänel's modification of the original van Leer scheme, it is obvious from fig. 4.9, that there is no significant qualitative difference with the solution using the van Leer scheme (fig. 4.1). However, due to the modification we expect an improvement of the preservation of total enthalpy. In fig 4.10 the total enthalpy along the stagnation streamline shows to be perfectly well preserved. The stagnation temperature is found to be $T_t = 4622K$ (theory $T_t = 4624.9K$). A substantial improvement compared to the original flux-vector splitting scheme is booked. A refinement of the mesh to 160x64 volumes shows that the stagnation temperature increases to $T_t = 4624.3K$. Again, the nose region flow shows no anomalies (fig. 4.11). Thus, it may be expected that further refinement yields an even more accurate stagnation temperature. As far as the preservation of total enthalpy is concerned, Hänel's scheme is preferred above van Leer's. The solution in the form of Mach contours (fig. 4.12) appears to be identical to the solution of MBB [9,10]. Compared to the scheme of van Leer, a less finer grid seems to be necessary to obtain an accurate solution with the Hänel scheme. The convergence is as good as with the van Leer scheme (fig. 4.13).

Both the van Leer scheme and the Hänel scheme perform well on the finest mesh considered (320x128 volumes). The Hänel scheme has the benefit of a slightly faster convergence and the perfectly preserved total enthalpy. This results in a stagnation temperature of $T_t = 4624.8K$ compared to $T_t = 4706.5K$ for the van Leer splitting scheme. The shock stand-off distance decreases to x/r=0.518 (fig. 4.14). The complete solution is shown in the form of Mach contours in fig. 4.15. The convergence history is plotted in fig. 4.16. The codes consume about 111 secs. of CPU time for 1000 integration steps on 40960 volumes.

A test of the robustness of the schemes by means of an increase of the CFL number to 0.75, forced the schemes of van Leer and Hänel to become unstable. The temperature and pressure became negative as the increase of CFL number was performed. Despite the modification of Hänel with respect to speed of sound, the flux still depends on the pressure, and the robustness does not seem to be improved compared with the original van Leer scheme. When the schemes were stable no advantage revealed of the modified scheme, at least for the test case considered.

A completely different experience is obtained with the Roe scheme. Fig. 4.17 shows the Mach contour plot of the solution on the 80x32 mesh. The solution shows to be qualitatively identical to those obtained with the van Leer and the Hänel scheme. The total temperature is found to be $T_t = 4890K$ which is worse than the van Leer scheme. The preservation of total enthalpy along the stagnation streamline is shown in fig. 4.18. It is obvious that the shock is captured in only one interior zone, though it seems (fig. 4.19) that only two states form the shock and are connected to each other through a discontinuity having no interior point. The shock stand-off distance on the coarse mesh is more accurate than the van Leer or the Hänel scheme (x/r=0.551) when compared with the MBB result. With respect to CPU time consumption the Roe scheme is slightly less efficient compared to the other schemes. The convergence is comparable (fig. 4.20).

In contrast to the solution with the Roe scheme on the 80x32 mesh which is almost identical to the solution using the flux-vector splitting, the solution on the 160x64 mesh reveals a completely unexpected behaviour. Fig. 4.21 shows the Mach contours of the solution using the Roe scheme on the 160x64 mesh. It is obvious that there is no physical relevance in the solution. The flow appears to be entirely unsymmetrical (fig. 4.22). No converge is achieved (fig. 4.23).

Problems concerning the convergence for hypersonic blunt body flows were reported by Yee [4]. She recommended to use an entropy-fix with a parameter controlled by the flow properties.

$$\Psi(z) = \begin{cases} |z| & |z| \geq \delta_1 \\ (z^2 + \delta_1^2)/2\delta_1 & |z| < \delta_1 \end{cases}$$

$$\delta_1 = \delta\left(\left| \frac{\tilde{u}}{\tilde{a}} \right| + \left| \frac{\tilde{v}}{\tilde{a}} \right| + 1 \right)$$

where $\Psi(z)$ is an entropy correction to $|z|$.

We applied an entropy-fix to the eigenvalues corresponding to shock wave structures, $|\tilde{u} - \tilde{a}|$ and $|\tilde{u} + \tilde{a}|$ in the above presented computations. The parameter controlling the amount of numerical viscosity added was chosen such that it depends on the local flow properties. On the 80x32 mesh $\delta = 0.05$ in order to avoid extensive smearing of the shock wave. On the finer 160x64 mesh, the parameter was increased to 0.20 to account for a less dissipative scheme on the finer mesh. It appeared to be insufficient. The shock outside the bulge is still captured with one interior zone.

The structure of the flow solution near the stagnation streamline may give an explanation of the appearance of the bulge upstream of the shock wave. Fig. 4.24 shows a velocity vector plot of the region near the symmetry line. It appears that a vortical flow has developed in the region between the shock wave and the nose of the body. Downstream of the shock wave in the plane of symmetry, the flow has reversed thus enabling the bulge to develop. Obviously, the scheme captures a shock wave which is too strong. It seems that the flow reversal initiates the asymmetry in the flow, probably due to the vanishing local velocity $\tilde{u}$.

The definition of the problem, the boundary conditions and also the method of solution do not give any motive for the development of an unsymmetrical flow pattern. Furthermore, it is odd that a mesh refinement leads to the unrealistic solution presented here. The same behaviour was also noticed for solutions obtained on the 80x32 grid with local refinements by means of a stretching of the grid (not shown here). The locally smaller mesh width seems to initiate this behaviour. In this case the calculation of thermodynamic quantities became erroneous. The flow reversal immediately downstream of the shock wave initiated negative temperature and pressure. This was not an issue with the flux-vector splitting schemes of both van Leer and Hänel.

A key to the origin of this problem may be found in the survey of Roberts [3]. He shows that a deficiency of the flux difference splitting methods is the noise generated downstream of a captured, slowly moving or nearly steady shock wave. He proves that a shock wave having one interior zone is not sufficiently viscous in a numerical sense to be able to damp the noise generated by an almost steady shock.

If we examine the convergence history (fig. 4.23) it seems reasonable to suppose that the shock does not become steady. The shock develops as the calculations proceed. It is first formed at the body surface and then slowly moves into the flow field where it should reach its 'equilibrium' position. Being not entirely steady, the shock wave may suffer from the aforecited deficiency. In this way we can actually understand the behaviour on the coarser mesh. The dissipation in the scheme also depends on the size of the mesh elements. The larger the cell size, the larger the local numerical dissipation; then, the scheme on the coarser mesh is sufficiently dissipative to damp the generated noise. This may explain the behaviour on the coarser mesh when local refinement is applied. It was also found that on a mesh of 40x16 volumes with local refinement an initially uniform solution converges to a symmetrical solution of the blunt body flow (not shown). This is in agreement with the former statement about the coarseness of the mesh.

Roberts showed in [3] that for one-dimensional problems, schemes that are continuously differentiable, smooth, and capable of capturing shocks with two interior zones, can effectively damp the noise generated by the downstream moving waves at nearly steady shocks. He also noted that in two-dimensions, especially when the shock is oblique to the mesh, the effect may be accentuated.

This can be a further explanation for the different behaviour of the Roe scheme in comparison with the flux-vector splitting schemes. The Roe scheme, unlike the other schemes considered, is not continuously differentiable. Continuous differentiability of the scheme guarantees a smoothness of the flux near sonic points, shock waves, and points where the velocity normal to the cell interface vanishes. Furthermore, the scheme captures shocks with at most one interior zone.

As mentioned before, Yee has reported problems concerning the convergence of hypersonic blunt body flows using the Roe scheme. She found an improvement by adding properly dosed numerical viscosity near shocks and sonic points. We modified the entropy-fix such that also near points where the velocity normal to the cell interface vanishes, some numerical viscosity is added to the eigenvalue $|\tilde{u}|$. The vanishing of this eigenvalue appeared to occur near very strong shock waves where the captured shock seems to be too strong. Fig. 4.25 shows the result of this modification on the 160x64 mesh by means of Mach contours, the bulge on the shock wave has disappeared. The flow field shows to be perfectly symmetric (fig. 4.26). It was found that the entropy parameter should be relatively large since a choice of 0.05 again leads to physically irrelevant solutions; we chose $\delta = 0.2$.

This result seems also a confirmation of the observations by Roberts. By adding numerical viscosity at the point where $|\tilde{u}|$ vanishes, in this case near the shock, the noise generated by the slowly moving shock is damped considerably better. The shock appears to be captured with two interior zones (fig. 4.27). The scheme offers a smoother transition near sonic points, shock waves and point where $|\tilde{u}|$ vanishes, though it is not continuously differentiable; also the convergence is retained (fig. 4.28).

It appears however, that, considering the sensitivity of the Roe scheme with respect to the amount of the numerical dissipation added, it is less appropriate for obtaining robust and trustworthy hypersonic blunt body flow solutions. This statement is confirmed by a computation of the flow on a mesh containing 160x64

volumes. The Roe scheme with the modified entropy correction but a smaller amount of numerical dissipation ($\delta = 0.05$) fails to converge. The solution is not symmetrical and the shock wave does not stabilize at its equilibrium position.

In fig. 4.29 the solution after 8000 integration steps on a mesh containing 320x128 volumes, achieved with the Roe scheme and the entropy correction parameter set to 0.20 is shown. The solution looks symmetric, however, a not entirely correct solution is seen in the nose region (fig. 4.29). A careful examination of the evolution of the solution leads to the conclusion that again a certain degree of asymmetry occurs. This behaviour can understood by looking at the shock structure. In fig. 4.30 it is observed that the scheme tends to capture the shock with only one interior zone. Although the convergence history shows an initially perfect convergence behaviour (fig. 4.31). Continuing the computations, however, shows that finally no convergence is achieved. The flow becomes asymmetrical as can be seen in the region near the symmetry line in a velocity vector plot (fig. 4.32).

A test run on the same grid (320x128 volumes) with the entropy parameter increased to 0.30 leads to a fully converged, perfectly symmetrical solution (fig. 4.33). During the integration process there is no sign of any asymmetry. The shock is captured with two interior zones, as expected (fig. 4.34). The stagnation temperature at the nose is $T_t = 4719.9K$. The shock stand-off distance is equal to the results obtained with the van Leer and the Hänel scheme: x/r=0.518. The scheme consumes 122 secs CPU time for each 1000 iterations. Again it has been found that the scheme must be sufficiently dissipative near shock waves in hypersonic flow to achieve a well-behaved solution.

The reason for the asymmetry of the flow solution may lie in the fact that the unsmoothness of the Roe scheme without a full entropy correction tends to yield stronger shocks with one interior point on fine meshes. Flow reversal can occur in these cases and a vortical flow pattern is formed. The scheme becomes ill-behaved due to the physical unreality. In all of the calculated problems using the Roe scheme with the modified entropy correction yet with insufficient numerical dissipation, the scheme tends to capture the shock in one interior point also. This results in a certain degree of asymmetry. On the coarser meshes the error in symmetry was eventually damped. The asymmetric behaviour is not entirely due to the hypervelocity effects, since a calculation of the Mach 2 flow past the hyperbola (not shown) did also reveal an unsymmetrical behaviour of the solution, although it was damped as the solution converged. It is typical for the Roe scheme and the influence depends on the actual damping capabilities of the scheme. The flux-splitting methods did not exhibit this malfunctioning.

Finally, it is worth noting that also the considered geometry of the problem can influence the course of the solution when using the Roe scheme. A first order computation of the Mach 25 frozen flow over a simple ellipse [11] was performed without an entropy correction (not shown here). During the computation some asymmetrical behaviour was observed but it was damped as the solution converged. Obviously, the mesh for the ellipse (200x50 volumes) offered sufficient dissipation near the shock. Furthermore, it may be that the shock was better aligned with the mesh.

5 Concluding remarks

In the present report a survey of three numerical flux functions is given. Each of the schemes are tested on a hypersonic blunt body flow with a free stream Mach number of 10.

It appeared that the flux-vector splitting of van Leer and the splitting of Hänel performed the best on the coarse and fine meshes with respect to robustness of the schemes.

The flux-difference scheme of Roe showed to be less robust for these types of aerodynamic problems since the robustness depends on an appropriate choice of the entropy correction parameter. With an inappropriate choice of this parameter the physically unrealistic solutions obtained on the finer meshes are in sharp contrast to the perfectly well behaved solutions realized with the flux splitting schemes. The need for a rather sophisticated entropy correction on all eigenvalues of the Roe-averaged Jacobian to achieve a higher degree of numerical dissipation does not argue for the scheme. In fact, it has been shown here that for the computation of hypersonic flows on fine meshes, the Roe scheme must capture strong shock waves with two interior zones in order to prevent the solution from becoming physically unrealistic.

The present results confirm the conclusion by Roberts that a scheme which captures steady shock waves in only one interior zone is not appropriate to use in explicit time-like marching schemes, where nearly stationary shocks can occur.

The performance of the flux splitting due to van Leer is negatively influenced by the fact that the preservation of enthalpy is not correct. The convergence of the schemes is satisfactory. Also the robustness appears to justify the choice of the schemes for the solution of hypersonic blunt body flows.

The modification of the original van Leer scheme as suggested by Hänel seems the best choice in solving hypersonic blunt body flow problems for a perfect gas. The preservation of enthalpy is perfect. The choice of the critical speed of sound instead of the statical speed of sound did not become apparent in the formulated test problem. At high CFL number the integration scheme showed to become unstable. The resulting negative thermodynamic quantities affect the correct performance of the scheme due to a dependence of pressure. For a stable scheme, it may be expected however, that when problems concerning the calculation of the speed of sound, and thus the performance of the splitting scheme, arise, the scheme due to Hänel shows a better behaviour.

The conclusion implies that in further research it is recommended to use the flux splitting methods in a generalized form such that flows of gases obeying an arbitrary equation of state can be computed. In this light we think of chemically reacting hypersonic flow in either thermal equilibrium or nonequilibrium. Examples of generalized flux splitting schemes may be found in literature.

Another aspect that arises with the flux splitting techniques is the poor resolution of contact discontinuities. A modification of the schemes is necessary in order to be able to capture contact discontinuities without an extensive smearing. Hänel gives such a modification in [8]. Therefore, it may pay off to modify the Roe scheme such that the total enthalpy is correctly preserved since the Roe scheme is able to correctly capture contact discontinuities. Then, an improvement of robustness could be achieved by more knowledge of the entropy correction and the resulting dissipative qualities of the scheme.

6 References

1. Spekreijse, S.P., Venis, A.C.J., "Numerical Evaluation of an Efficient Roe Scheme and Chemical Models for Chemically Reacting Nozzle Flows in Thermal Equilibrium", NLR TP90060 L

2. Hänel, D., Schwane, R., "On the Accuracy of Upwind Schemes for the Solution of Navier-Stokes Equations", AIAA-87-1105 CP

3. Roberts, T.W., "The behavior of Flux Difference Splitting Schemes near Slowly Moving Shock Waves", FFA TN 1988-58, The Aeronautical Research Institute of Sweden, Aerodynamics Department

4. Yee, H.C., "Upwind and Symmetric Shock-Capturing Schemes", NASA TM-89464

5. Spekreijse, S.P., "Multigrid Solution of the Steady Euler Equations", CWI tract 46, Centre for Mathematics and Computer Science

6. Roe, P.L., "Approximate Riemann Solvers, Parameter Vectors, and Difference Schemes", Journ. of Comp. Phys. 43, pp. 357-372 (1981)

7. van Leer, B., "Flux-Vector Splitting for the Euler Equations", Eight Int. Conf. on Num. Meth. in Fl. Dyn., Lec. Notes in Physics, 170, Ed. E. Krause, Springer Verlag, Berlin

8. Hänel, D., Schwane, R., "An Implicit Flux-Vector Splitting Scheme for the Computation of Viscous Hypersonic Flow", AIAA-89-0274

9. Eberle, A., Schmatz, M.A., Bissinger, N.C., "Generalized Flux Vectors fo Hypersonic Shock-Capturing", AIAA-900390

10. Schmatz, M.A., "Hypersonic Three-Dimensional Navier-Stokes Calculations for Equilibrium Gas", AIAA-89-2183

11 Workshop on Hypersonic Flows for Reentry Problems, January 22-25, 1990, Antibes (France), "Problem 6: Flow over an double/simple ellipse"

Figures

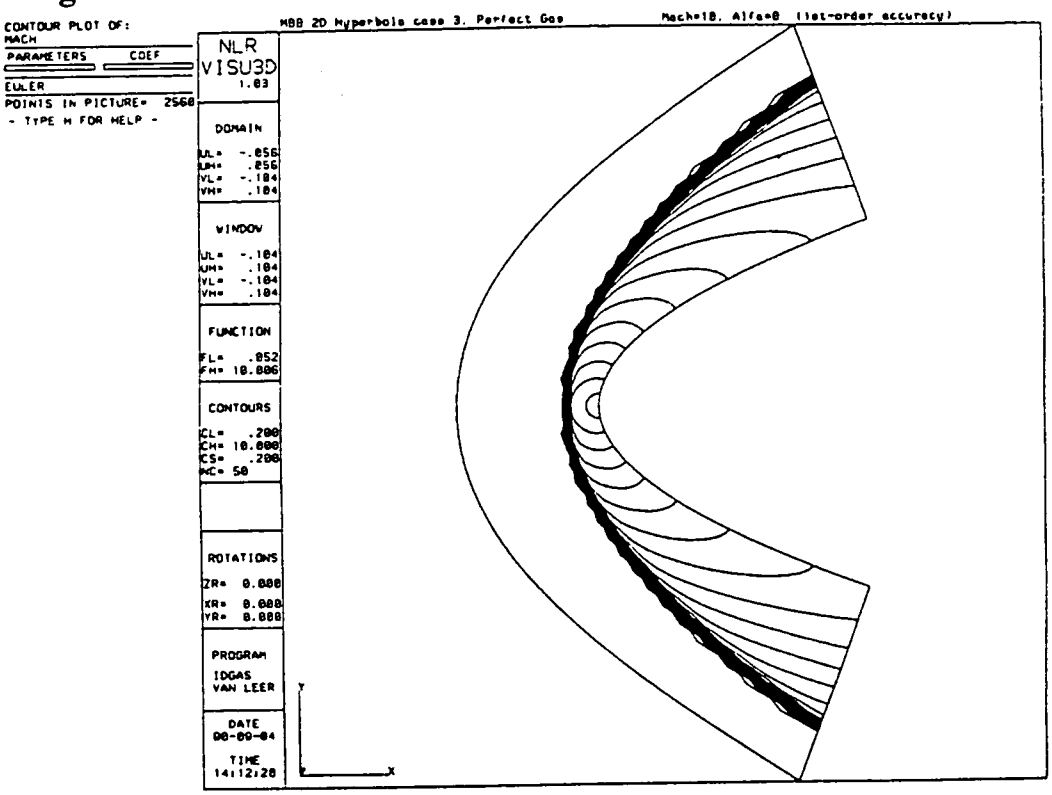

Fig. 4.1 Mach contours (van Leer scheme; grid: 80x32)

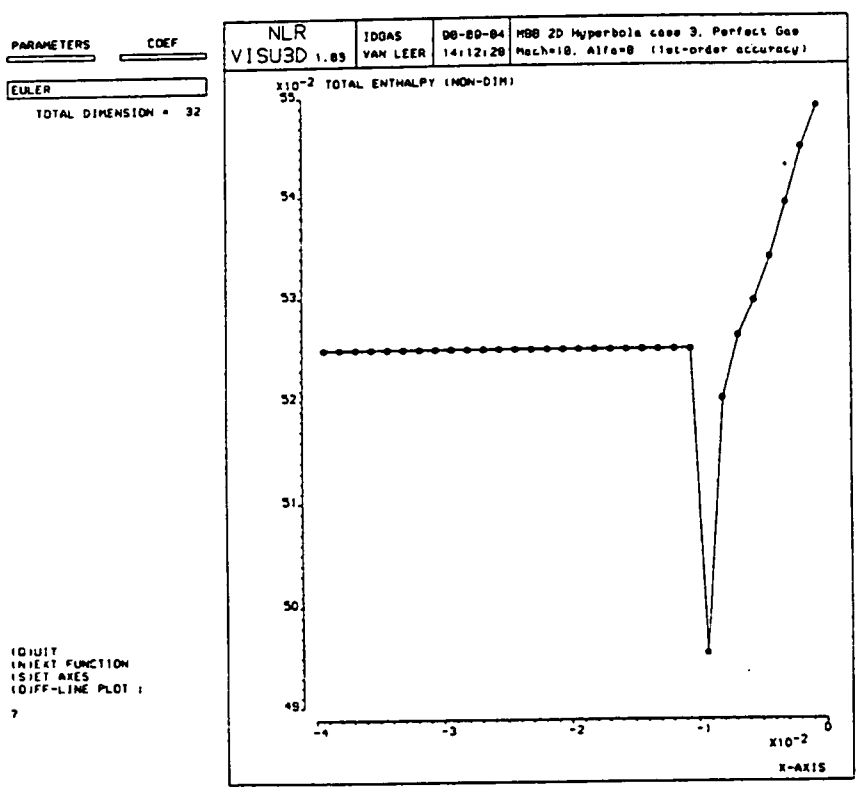

Fig. 4.2 Total enthalpy along stagnation streamline (van Leer scheme; grid 80x32)

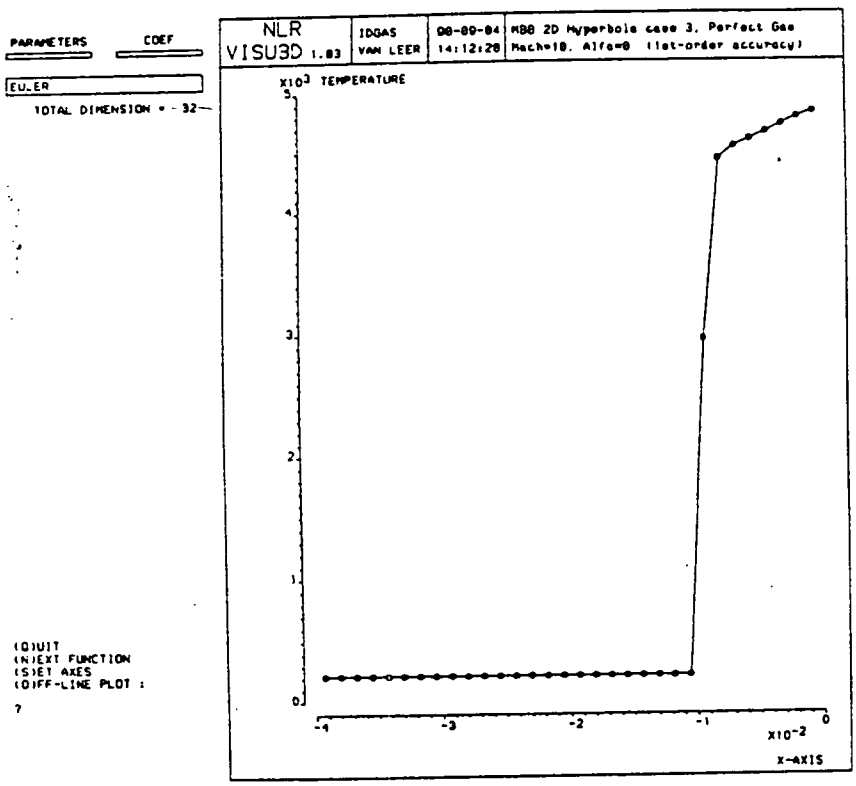

Fig. 4.3 Temperature along stagnation streamline (van Leer scheme; grid: 80x32)

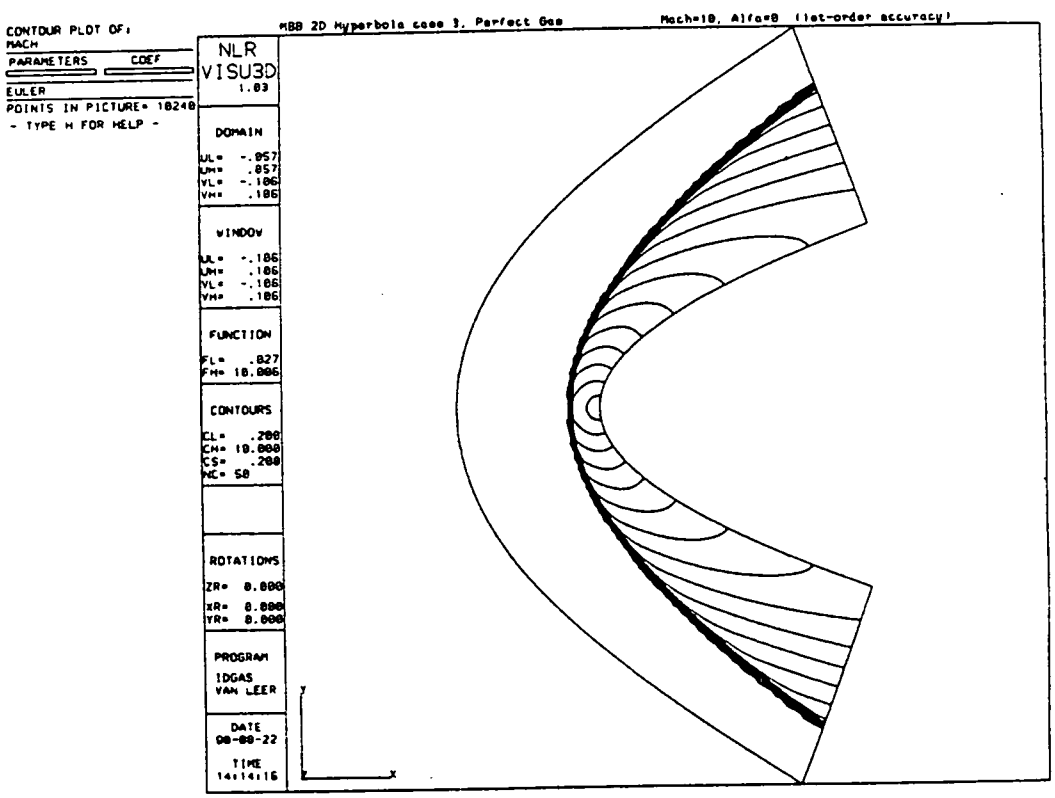

Fig. 4.4 Mach contours (van Leer scheme; grid: 160x64)

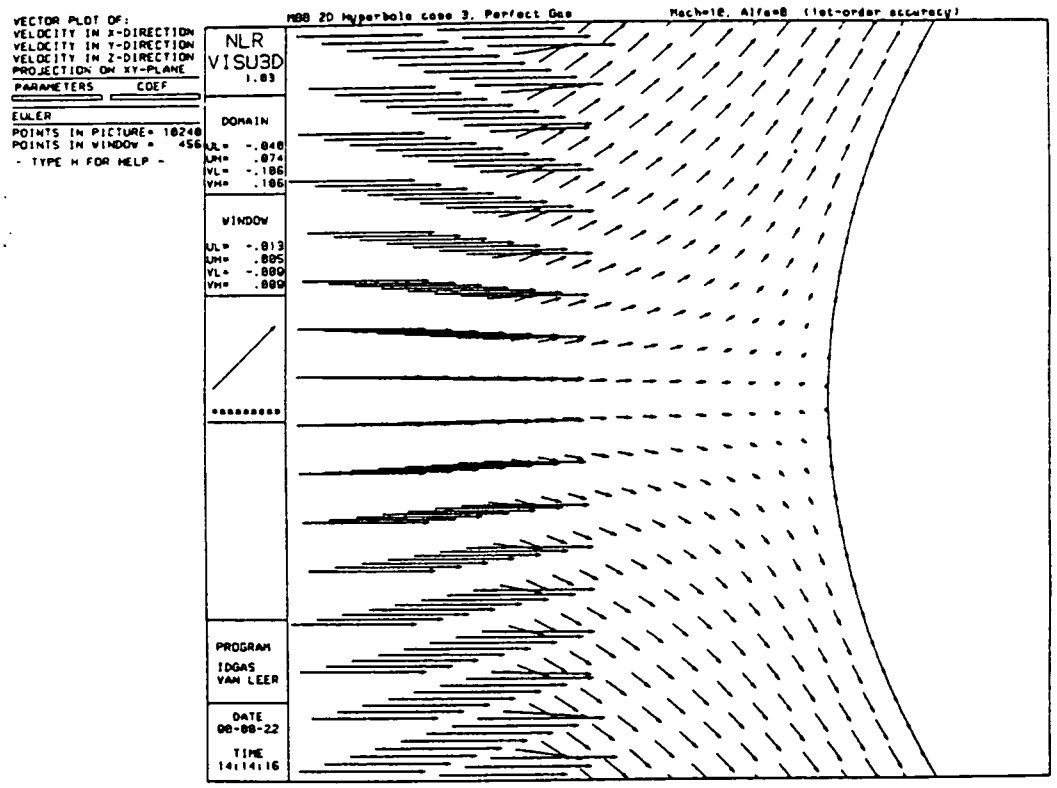

Fig. 4.5 Velocity vector plot of the nose region (van Leer scheme; grid: 160x64)

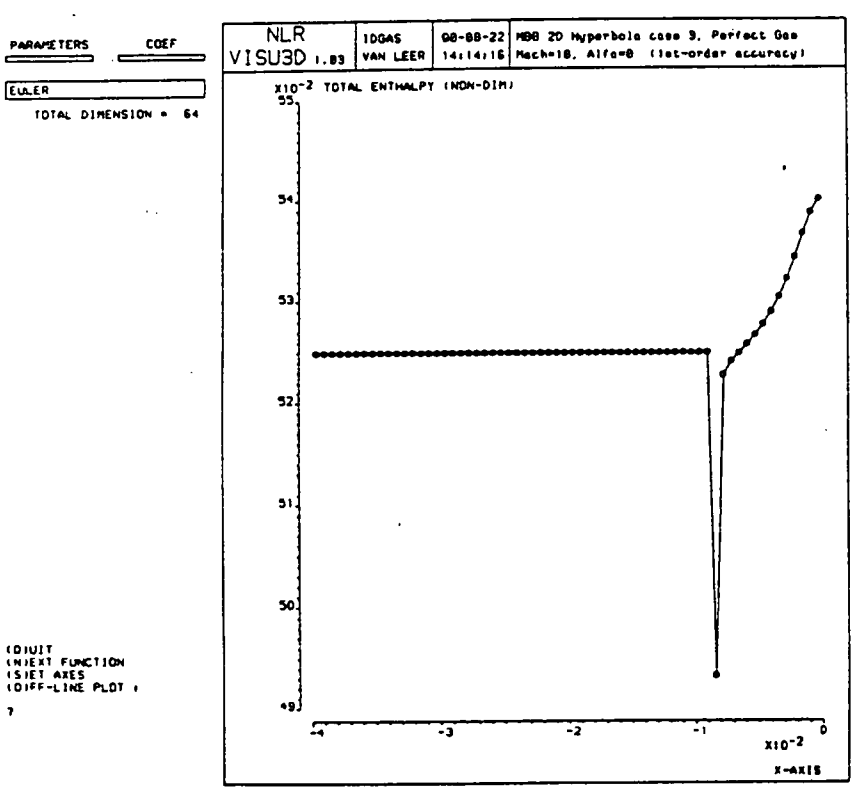

Fig. 4.6 Total enthalpy along stagnation streamline (van Leer scheme; grid: 160x64)

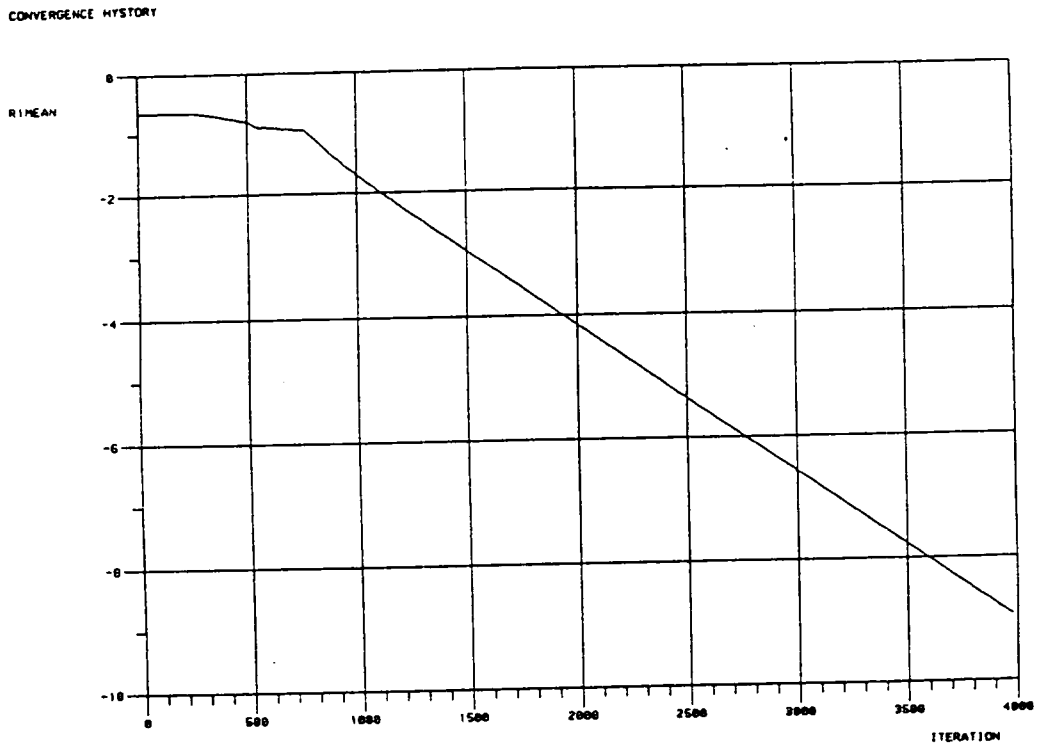

Fig. 4.7 Convergence history (van Leer scheme; grid: 80x32)

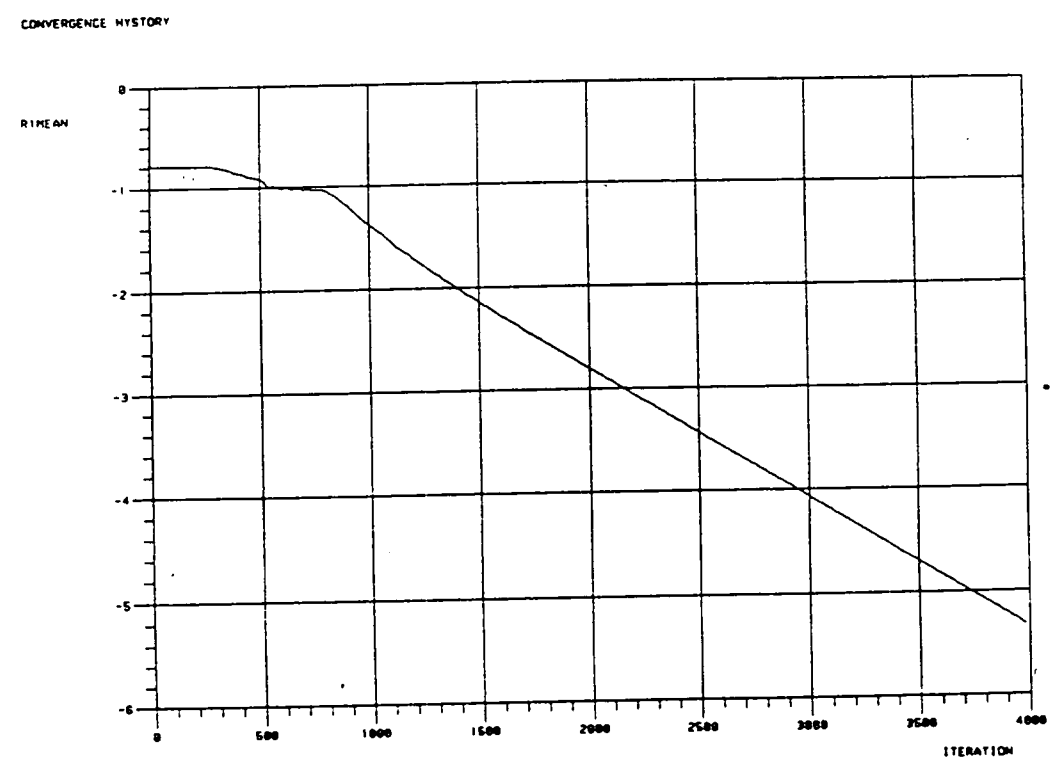

Fig. 4.8 Convergence history (van Leer scheme; grid 160x64)

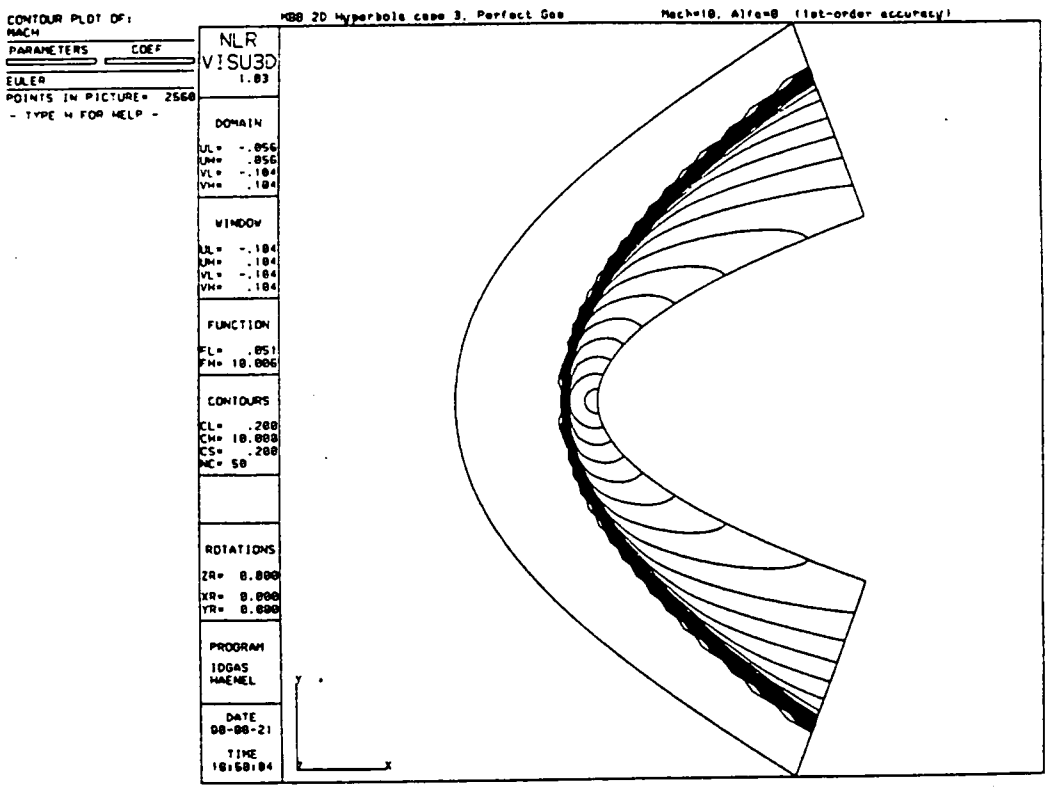

Fig. 4.9 Mach contours (Hänel's scheme; grid: 80x32)

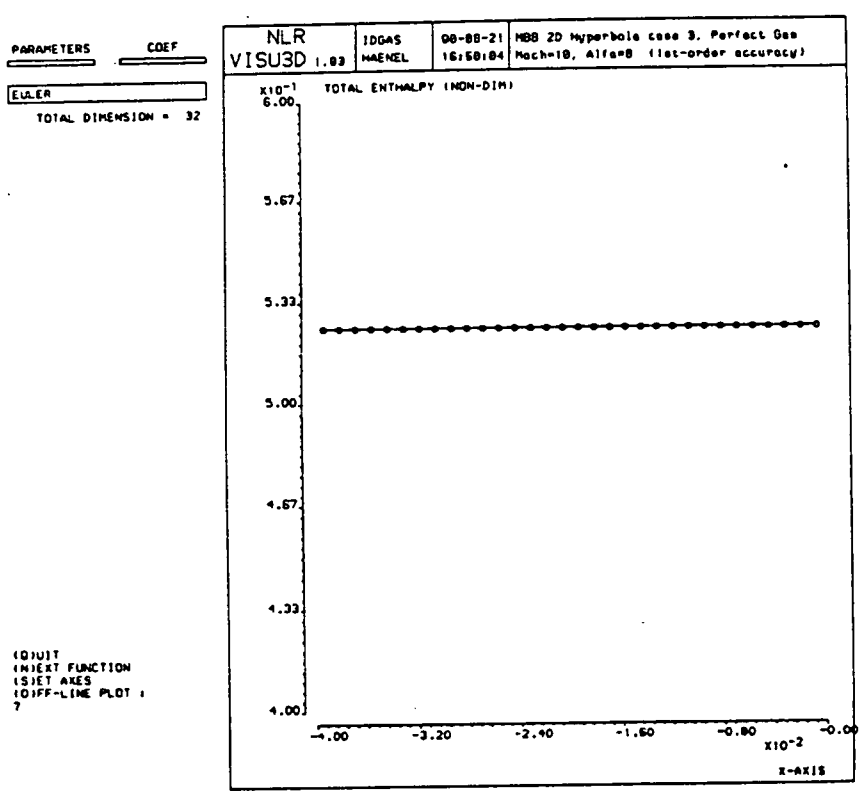

Fig. 4.10 Total enthalpy along stagnation streamline (Hänel's scheme; grid 80x32)

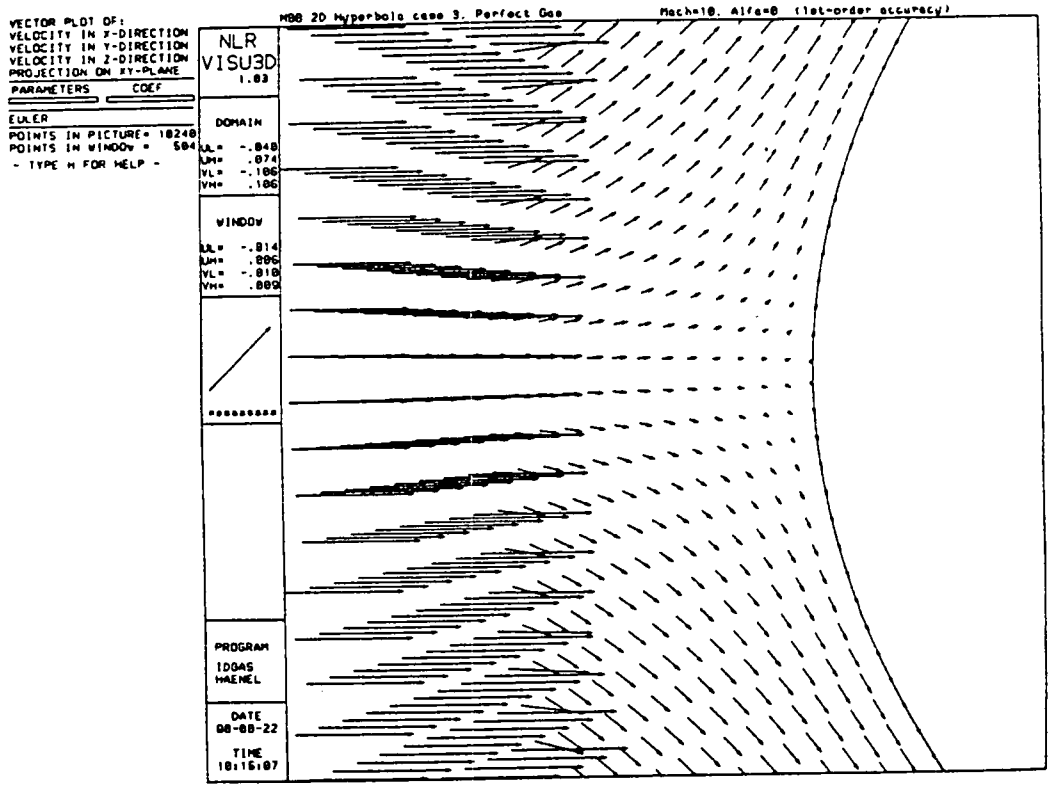

Fig. 4.11 Velocity vector plot of the nose region (Hänel's scheme; grid: 160x64)

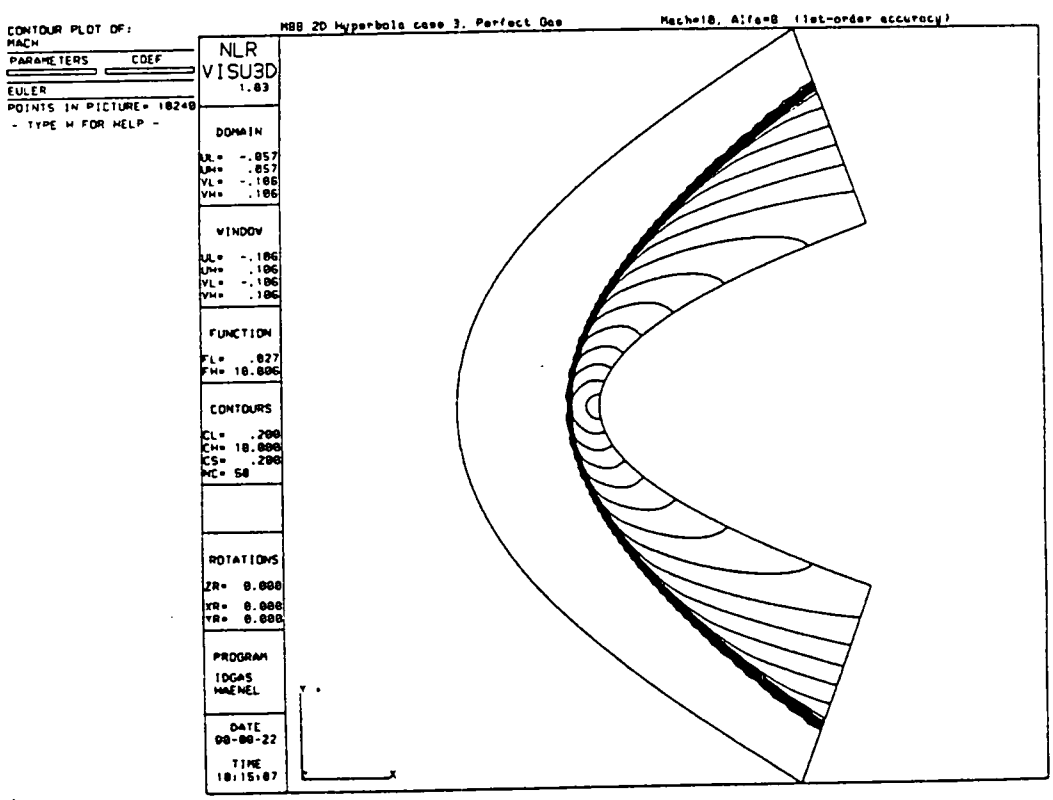

Fig. 4.12 Mach contours (Hänel's scheme; grid: 160x64)

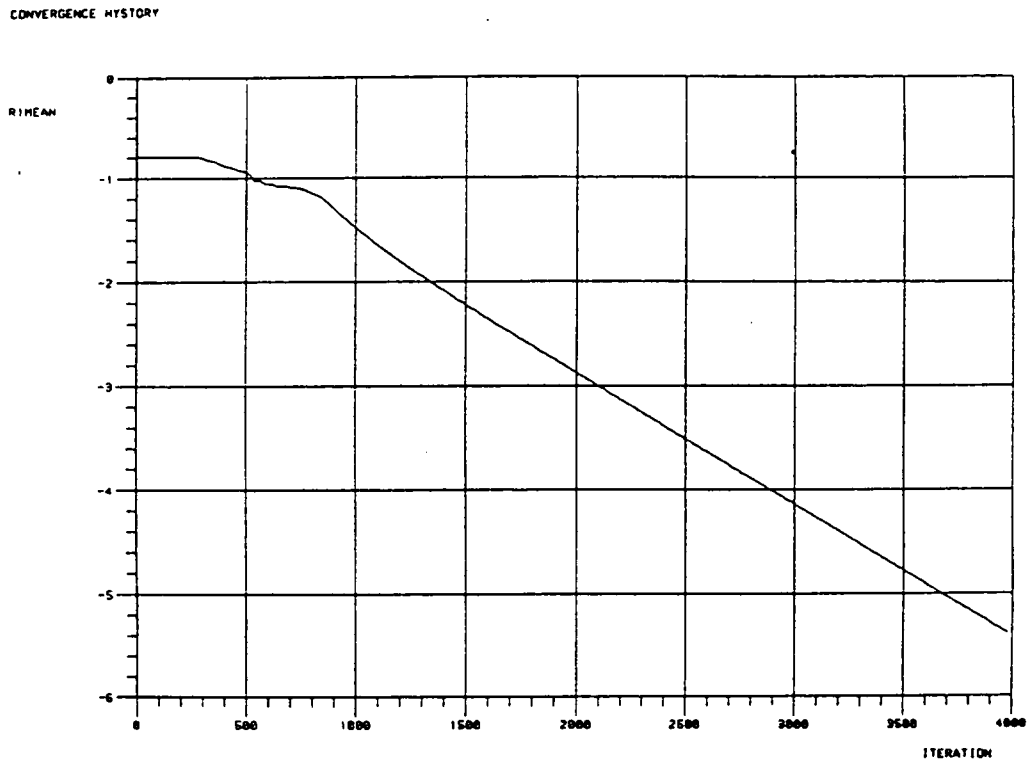

Fig. 4.13 Convergence history (Hänel's scheme; grid: 160x64)

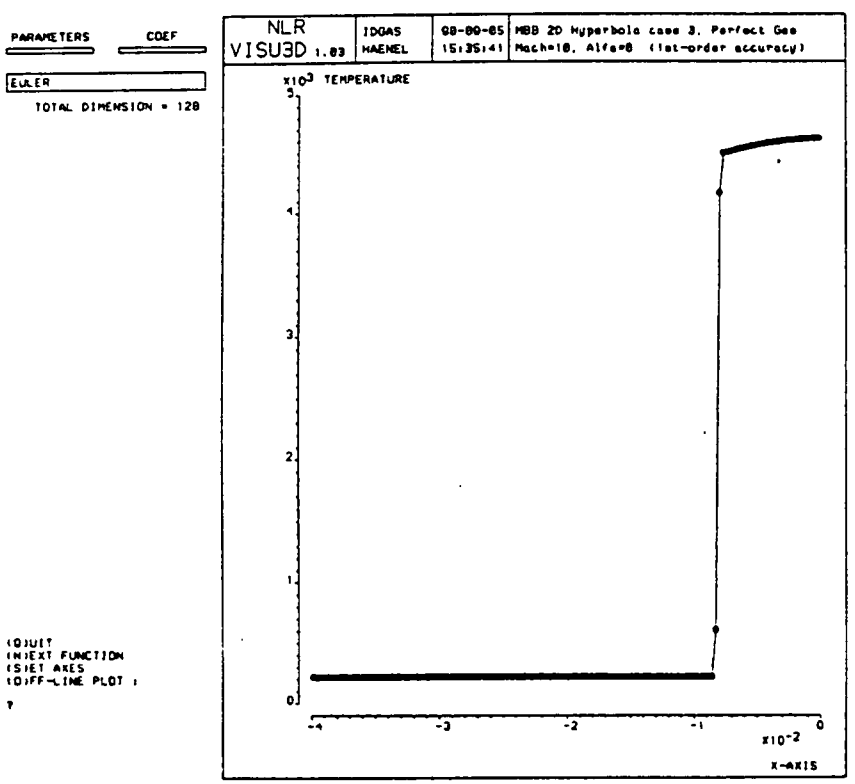

Fig. 4.14 Temperature along stagnation streamline (Hänel's scheme; grid: 320x128)

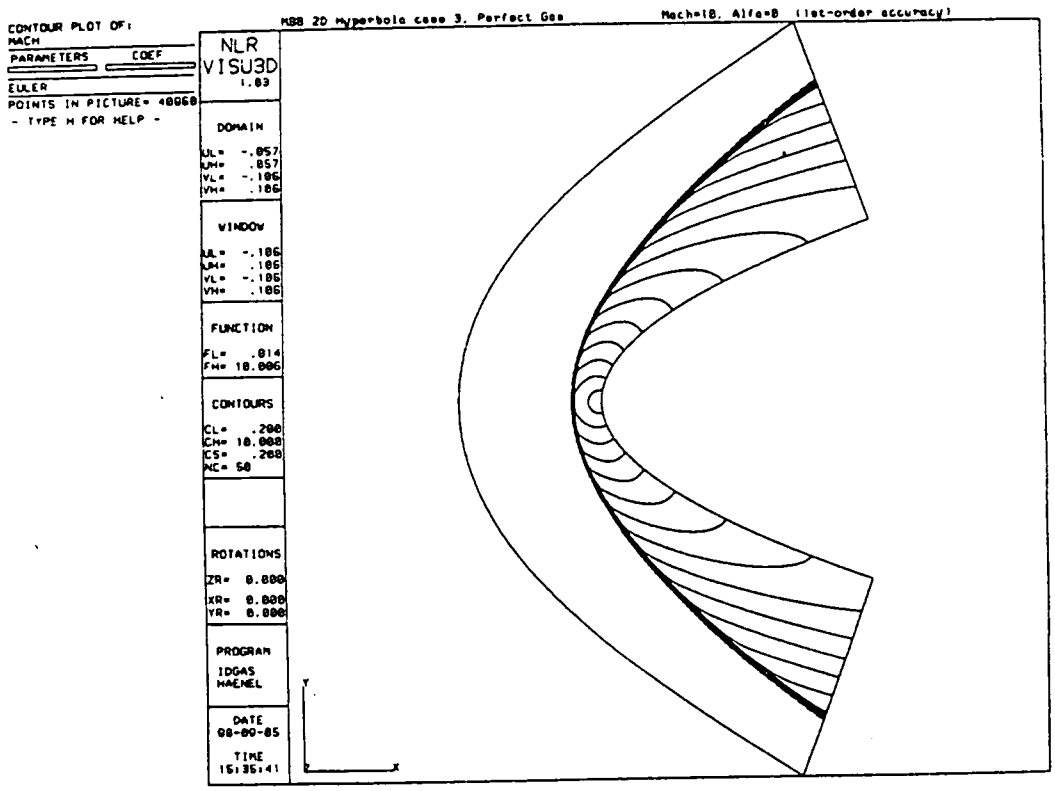

Fig. 4.15 Mach contours (Hänel's scheme; grid: 320x128)

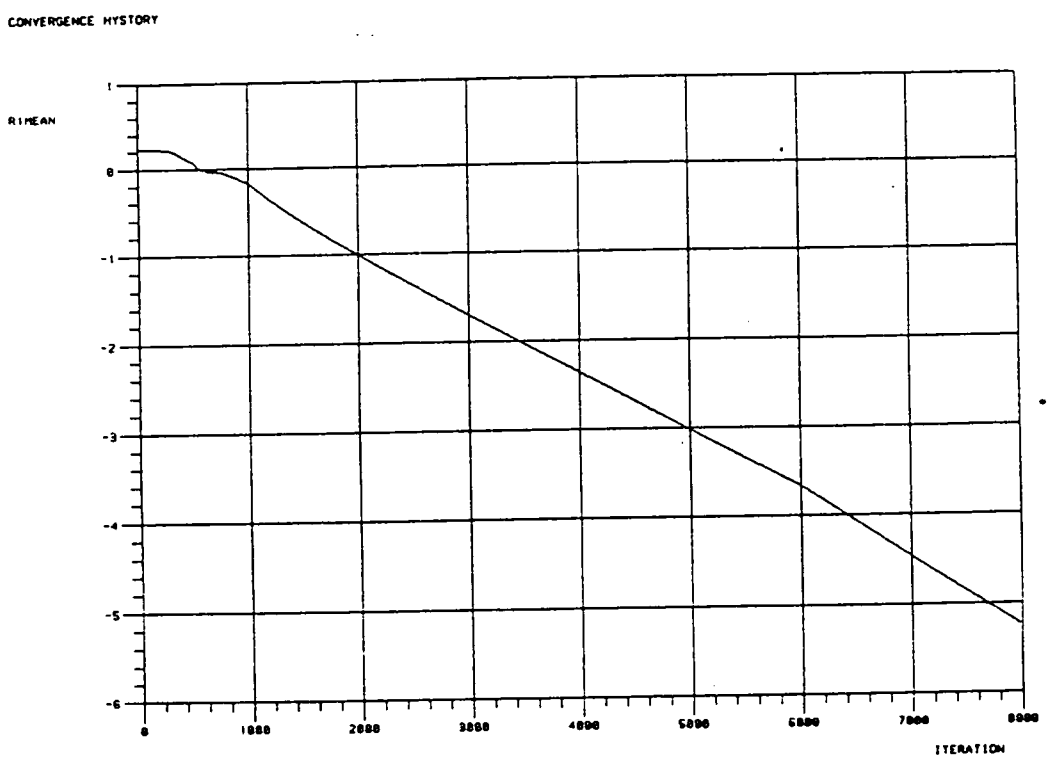

Fig. 4.16 Convergence history (Hänel's scheme; grid: 320x128)

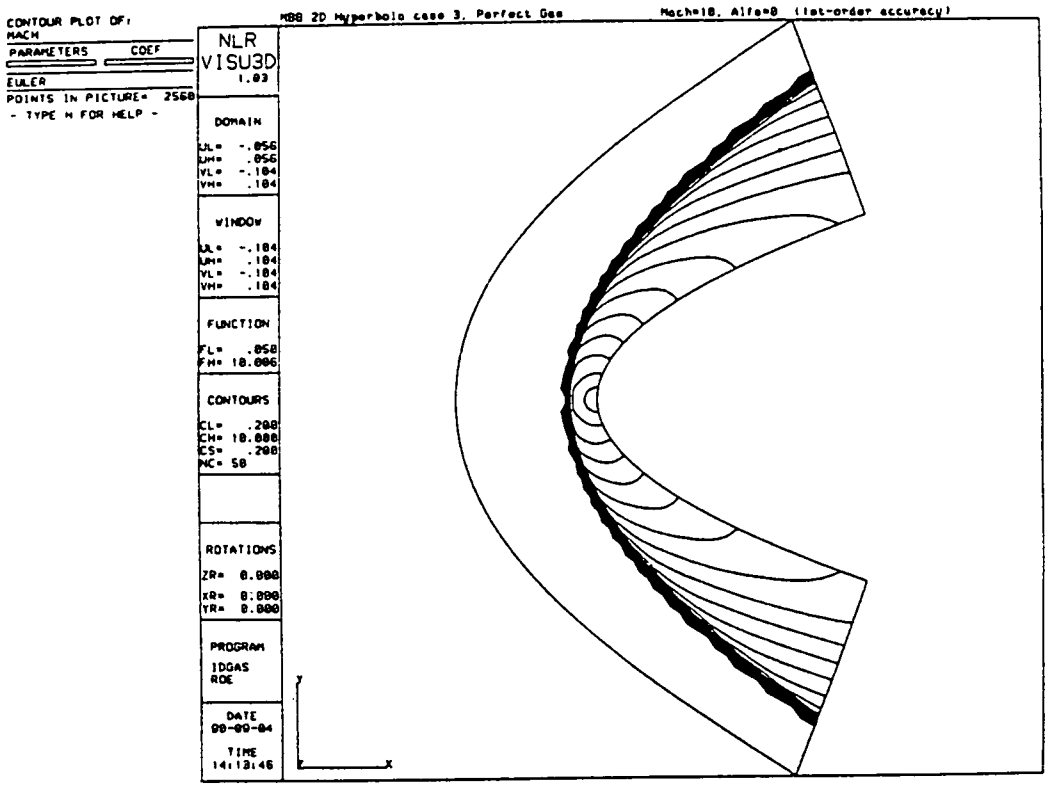

Fig. 4.17 Mach contours (Roe scheme; grid: 80x32)

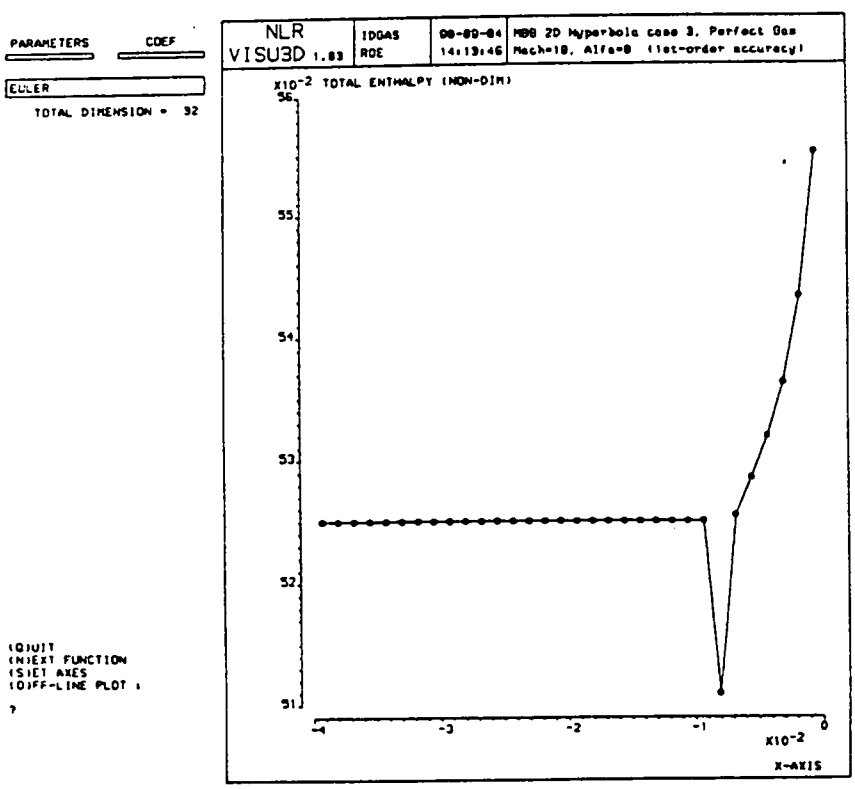

Fig. 4.18 Total enthalpy along stagnation streamline (Roe scheme; grid: 80x32)

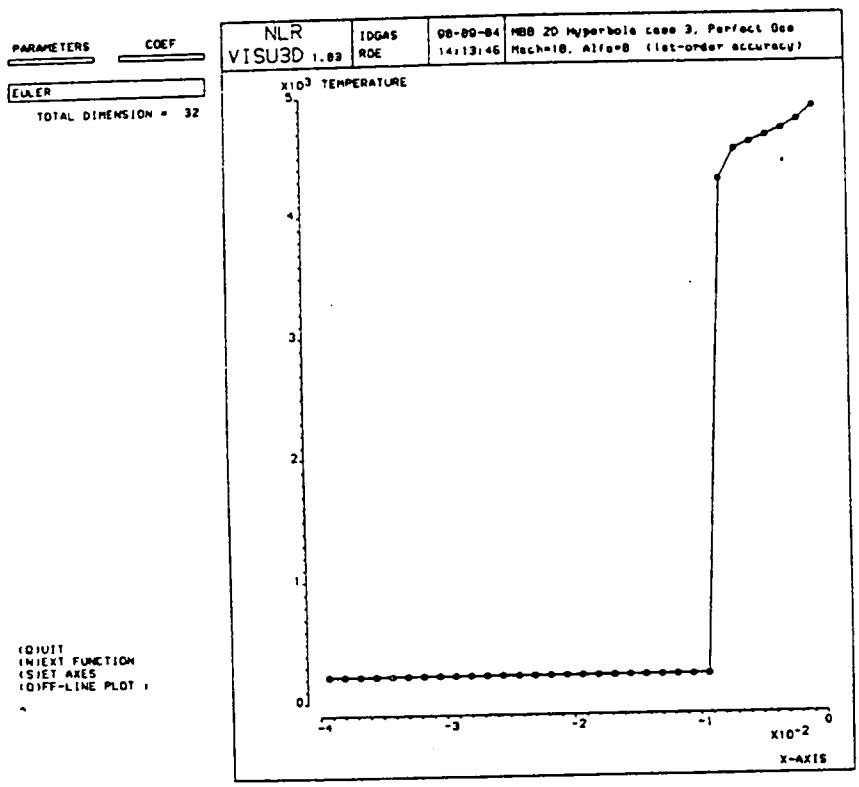

Fig. 4.19 Temperature along stagnation streamline (Roe scheme; grid 80x32)

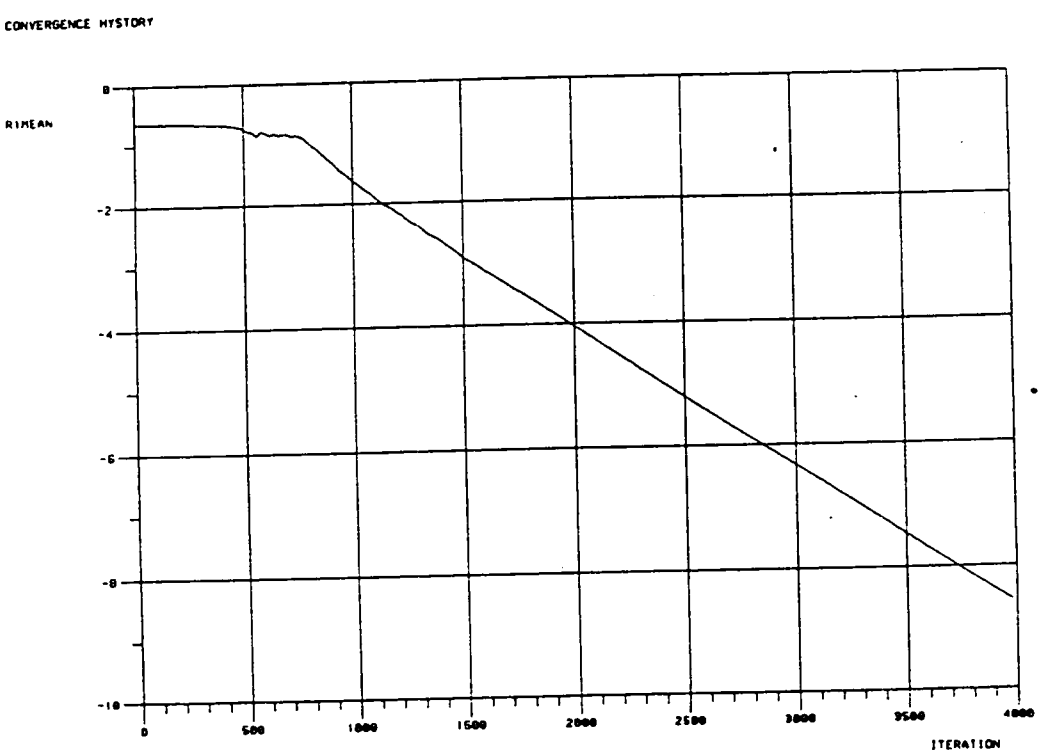

Fig. 4.20 Convergence history (Roe scheme; grid: 80x32)

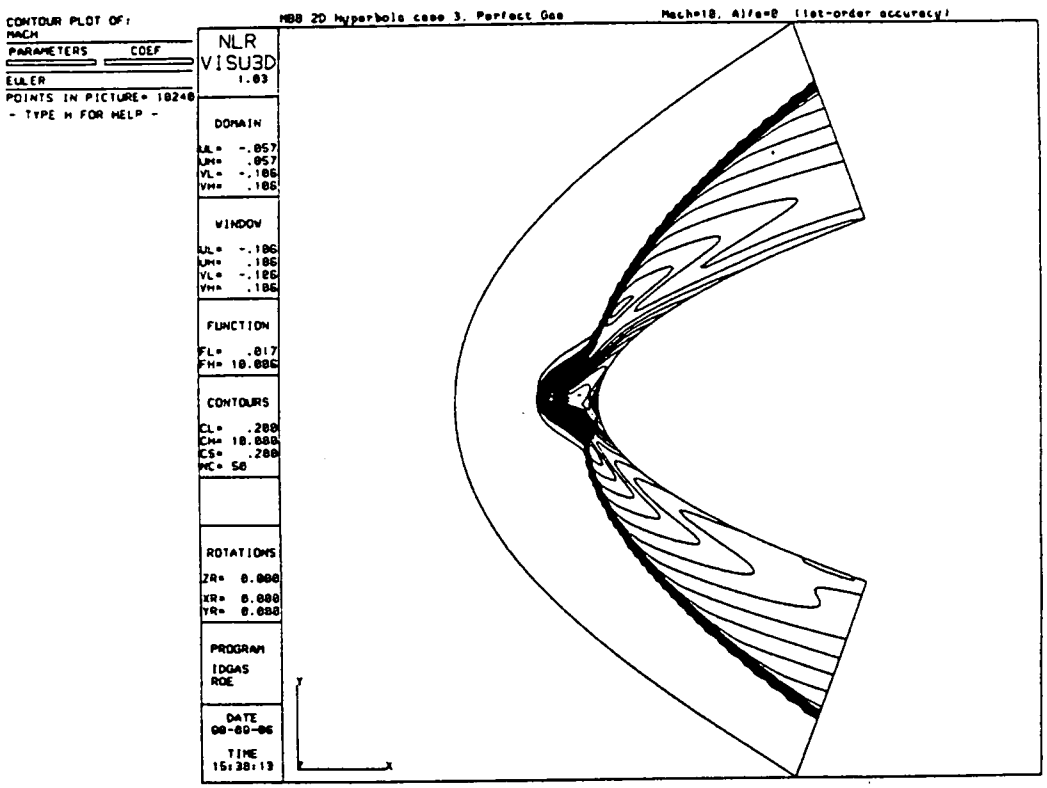

Fig. 4.21 Mach contours (Roe scheme; grid: 160x64)

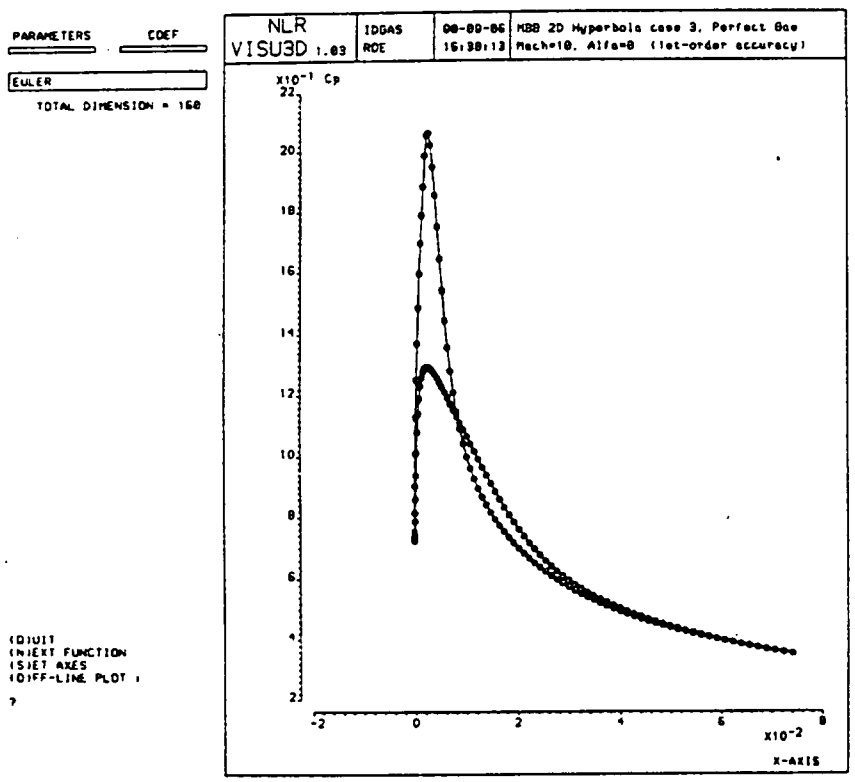

Fig. 4.22 Cp along body surface (Roe scheme; grid: 160x64)

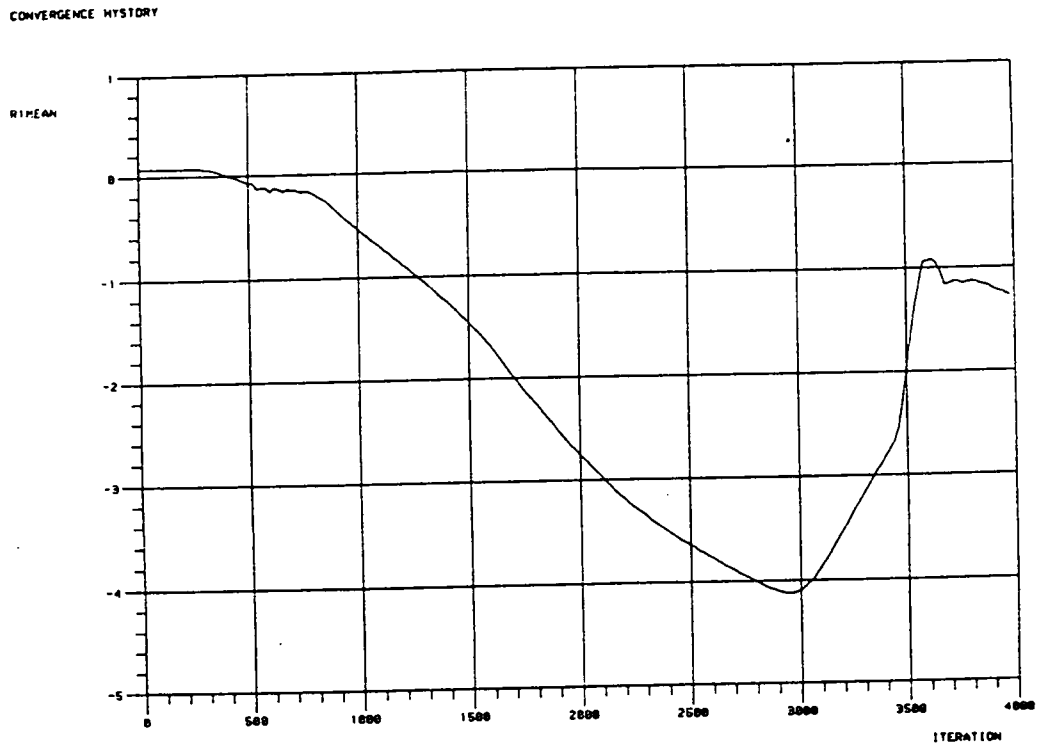

Fig. 4.23 Convergence history (Roe scheme; grid: 160x64)

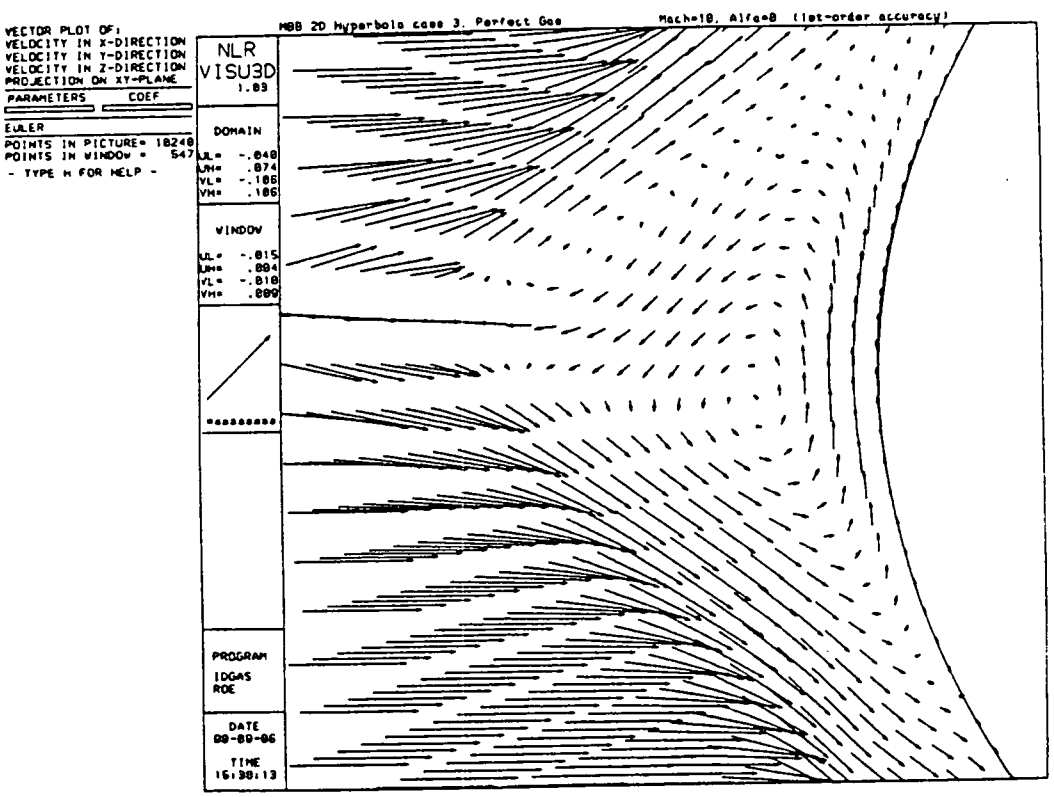

Fig. 4.24 Velocity vector plot of the nose region (Roe scheme; grid: 160x64)

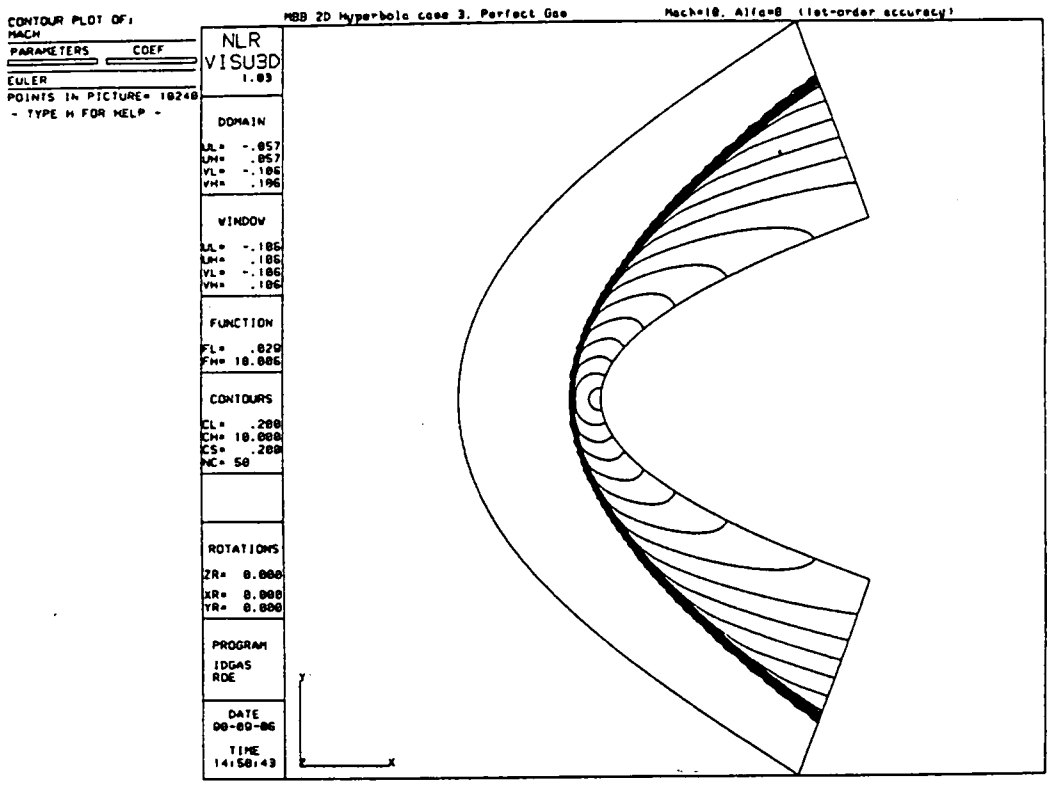

Fig. 4.25 Mach contours (Roe scheme, modified entropy fix; grid: 160x64)

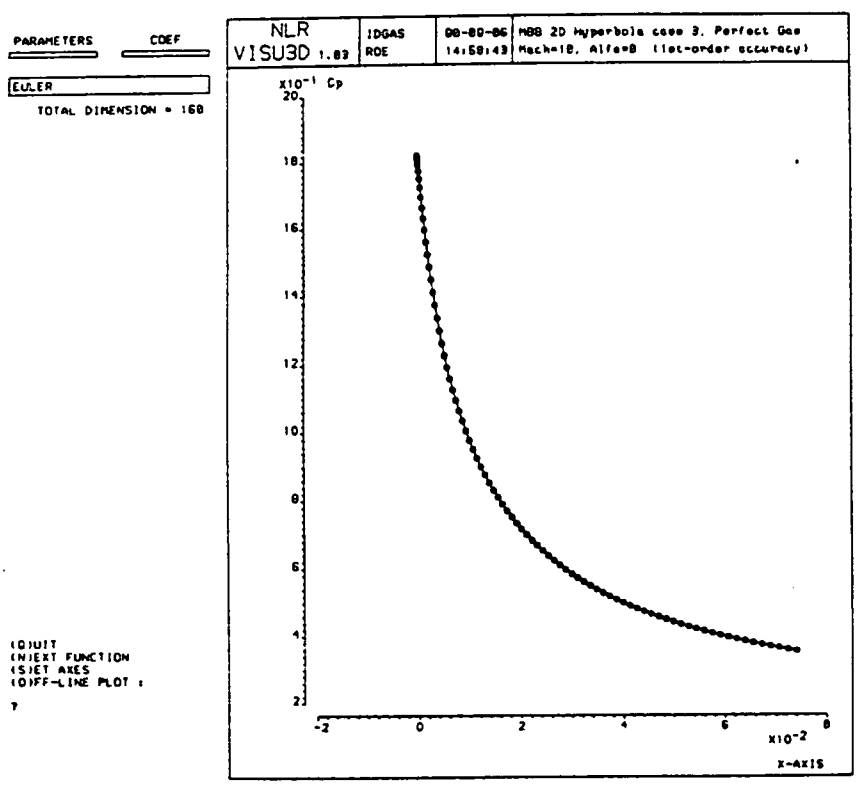

Fig. 4.26 Cp along body surface (Roe scheme, modified entropy fix; grid: 160x64)

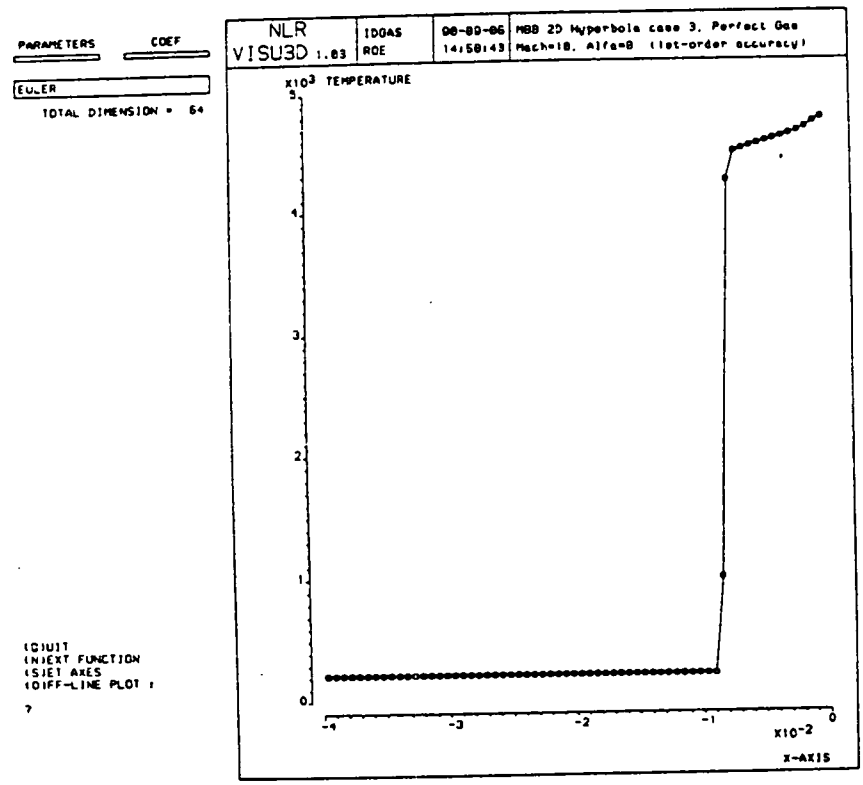

Fig. 4.27 Temperature along stagnation streamline (Roe scheme, modified entropy fix; grid: 160x64)

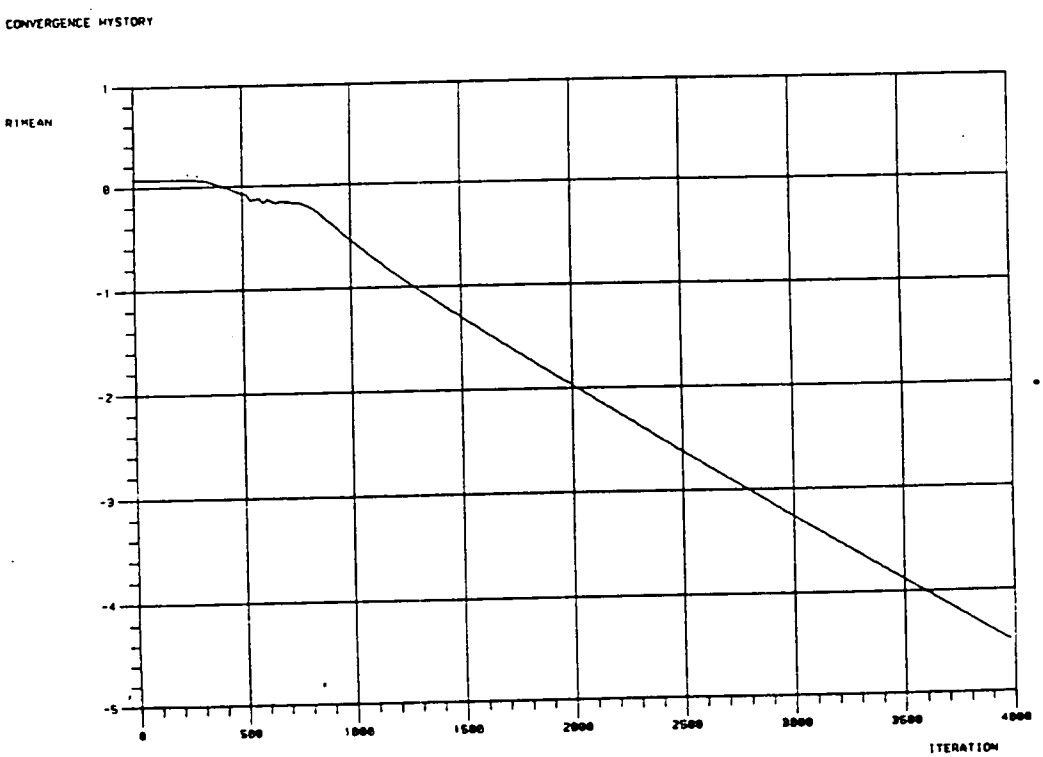

Fig. 4.28 Convergence history (Roe scheme, modified entropy fix; grid: 160x64)

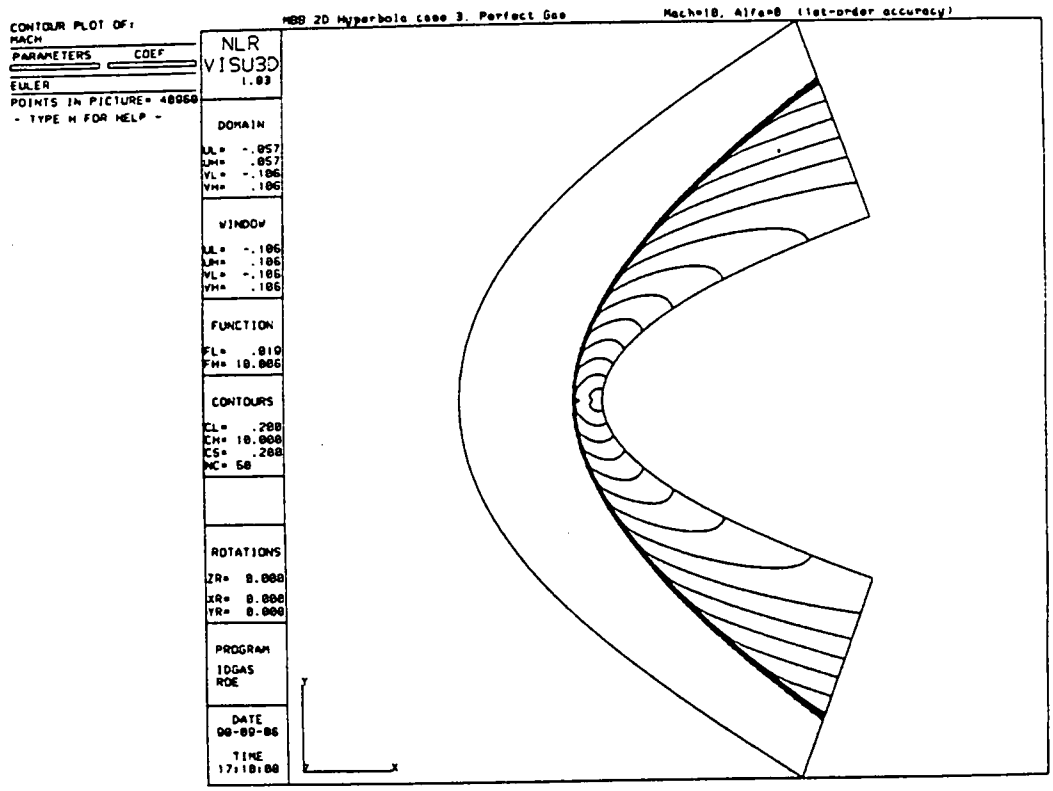

Fig. 4.29 Mach contours (Roe scheme, modified entropy fix, δ = 0.2; grid: 320x128)

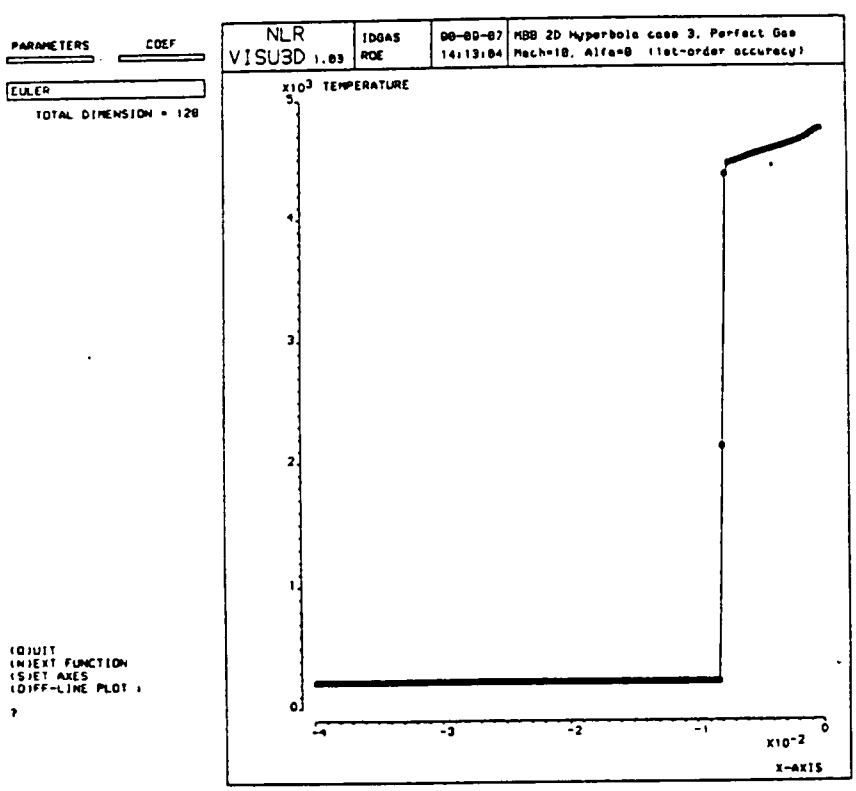

Fig. 4.30 Temperature along stagnation streamline (Roe scheme, modified entropy fix, δ = 0.2; grid: 320x128)

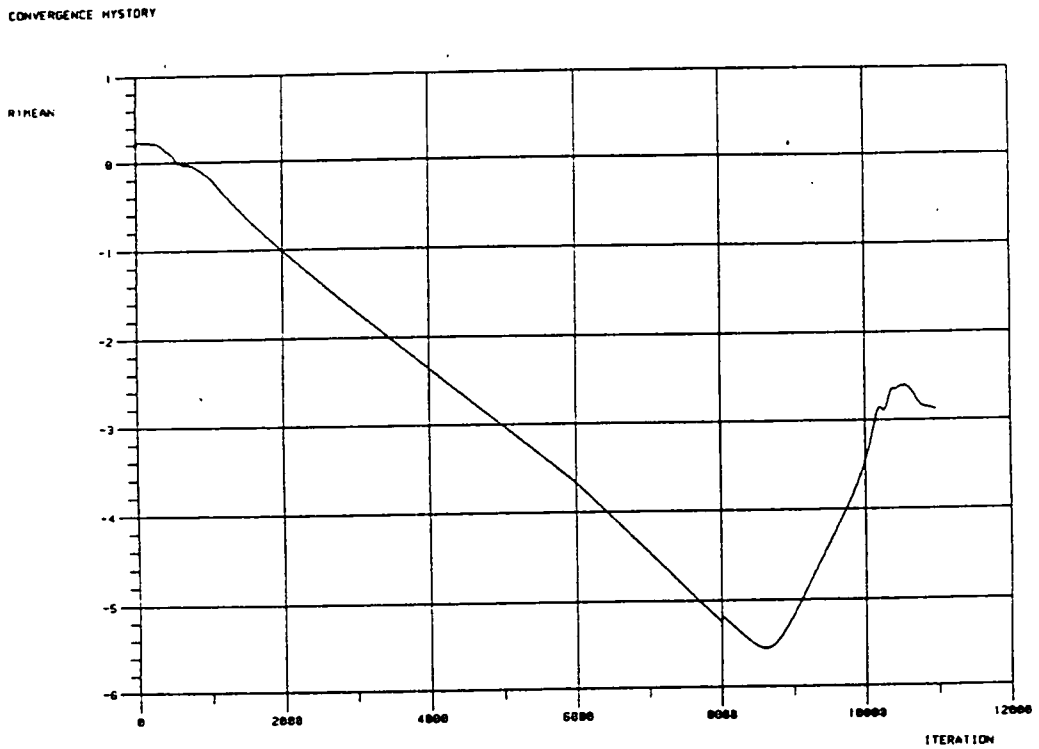

Fig. 4.31 Convergence history (Roe scheme, modified entropy fix, δ = 0.2; grid: 320x128)

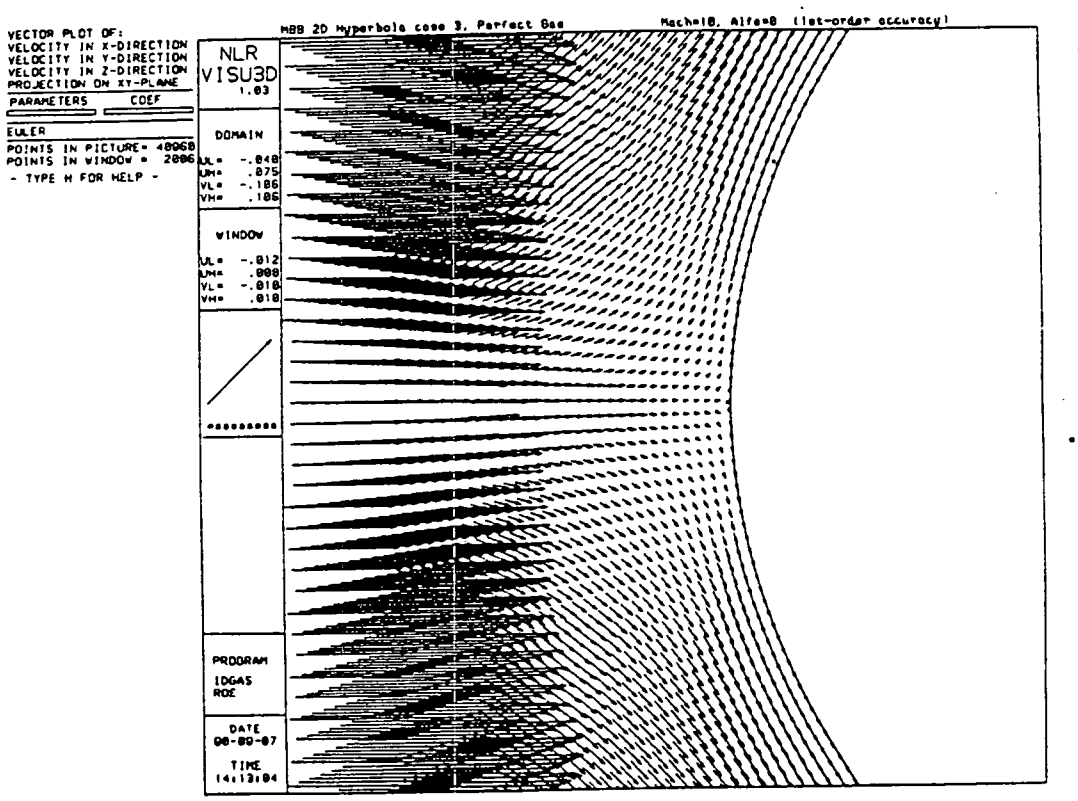

Fig. 4.32 Velocity vector plot of the nose region (Roe scheme, modified entropy fix, δ = 0.2; grid: 320x128)

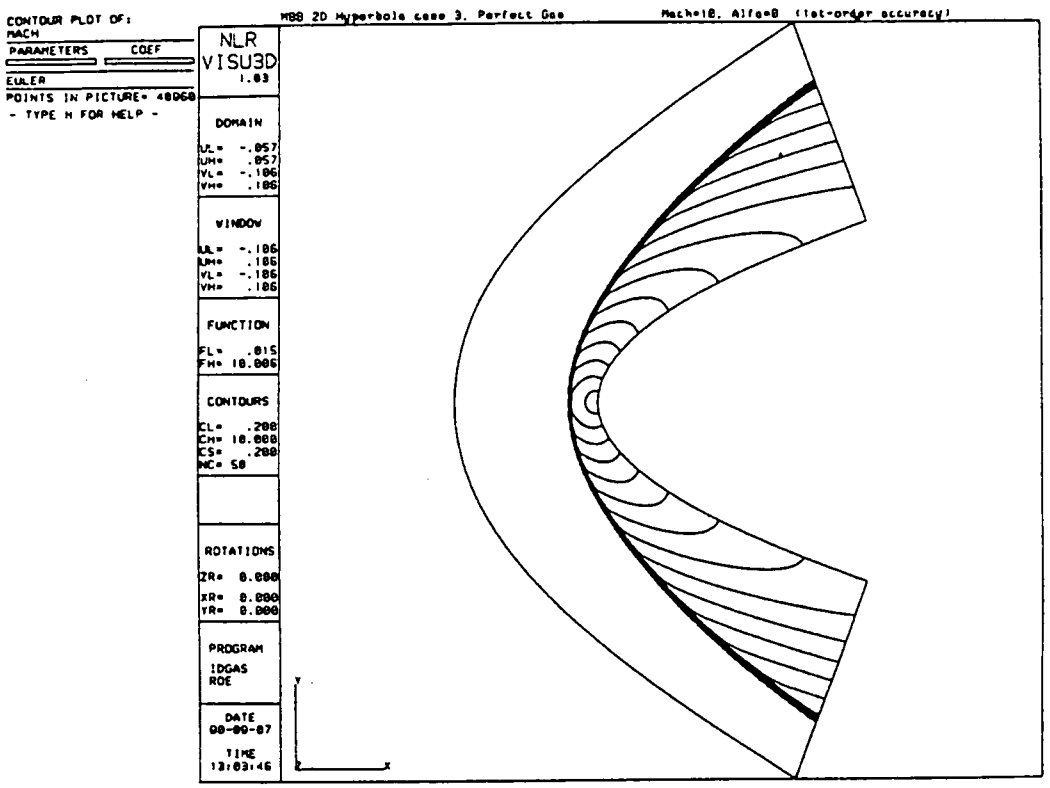

Fig. 4.33 Mach contours (Roe scheme, modified entropy fix, δ = 0.3; grid: 320x128)

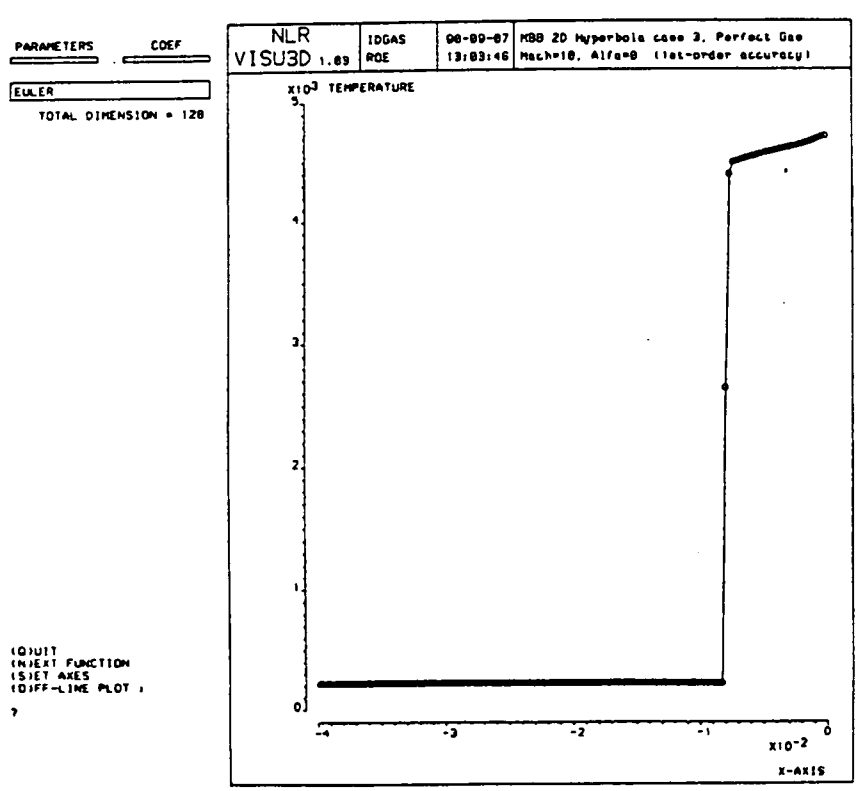

Fig. 4.34 Temperature along stagnation streamline (Roe scheme, modified entropy fix, δ = 0.3; grid: 320x128)